Supporting Information for:

Avoiding and Reducing Microplastic False Positives from Dry Glove Contact

Madeline E. Clough,[a] Eduardo Ochoa Rivera,[b] Abbygail M. Ayala,[a] Rebecca L. Parham,[a] Joseph Pennacchio,[b] Henry E. Thurber,[c] Andrew P. Ault,[a] Ambuj Tewari,[b,d] and Anne J. McNeil[a,c,e*]

[a]*Department of Chemistry, University of Michigan, Ann Arbor, MI 48109-1055, USA*

[b]*Department of Statistics, University of Michigan, Ann Arbor, MI 48109-1107, USA*

[c]*Macromolecular Science and Engineering Program, University of Michigan, Ann Arbor, MI 48109-2102, USA*

[d]*Department of Electrical Engineering and Computer Science, University of Michigan, Ann Arbor, MI 48109-2122, USA*

[e]*Program in the Environment, University of Michigan, Ann Arbor, MI 48109-1041, USA*

Table of Contents

I. Establishing a baseline of current glove recommendations

Two Web of Science topic searches were conducted in December 2023 and October 2024 for keywords 1) “microplastic*” and “quality assurance”, 2) “microplastic*” and “quality control”, and 3) “microplastic*” and “best practices”. The results of each search were pooled and duplicate publications were discarded. Then, the remaining articles were filtered to only include reviews. For each article, keywords “hand” and “glove” were searched, and recommendations on glove use and material were recorded. Where no mention of either keyword was found, the article was removed from consideration. Based on this protocol, 26 reviews were analyzed to obtain results.

The impact of the Witzig et al. article, which first illustrated that glove leachates can cause MP false positives in aqueous systems, was evaluated by comparing the recommendations of publications published before and after the article (post-2020).

Prior to the 2020 publication, glove use was largely recommended. After the publication, the proportion of reviews that do not recommend glove use increased by 7% (Figure S1). Beyond the 2020 article, the recommendations for latex glove material increased by 30% (Figure S2). The uptick in latex recommendations is a hypothesized result of the sample selection performed in the Witzig et al. article, where seven nitrile brands were compared to a single latex example, although both materials exhibited similar rates of MP false positives.[1]

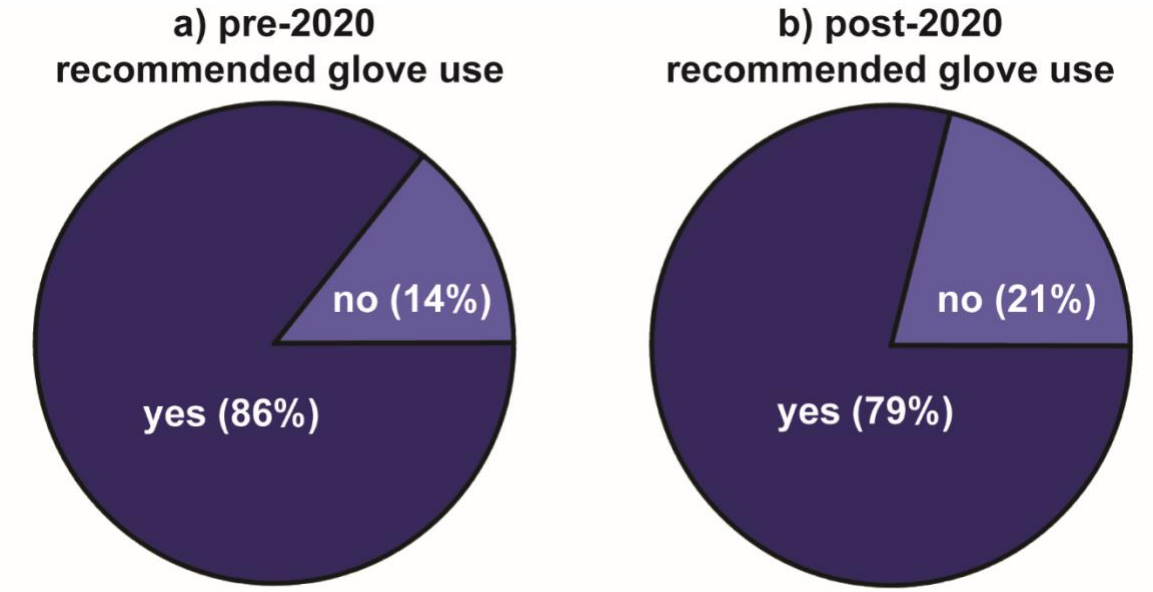

Figure S1. Literature search summary of recommended glove use (a) pre-Witzig et al. publication (N = 7) and (b) post-Witzig et al. publication (N = 19).

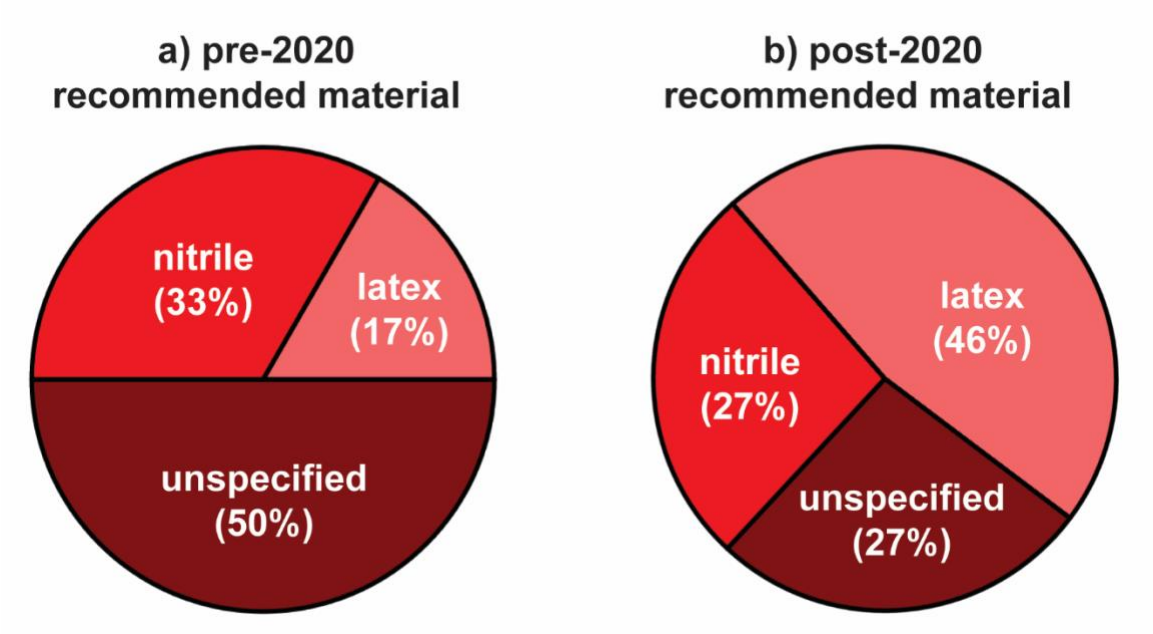

Figure S2. Literature search summary of the reviews that recommended glove use (a) pre-Witzig et al. publication (N = 6) and (b) post-Witzig et al. publication (N = 15).

II. Selecting laboratory gloves

In total, seven glove types were selected for analysis. Each glove was rated for chemical use, powder-free, and textured. Three gloves were latex material, three gloves were nitrile material, and one glove was a clean-room rated particulate-free nitrile material (Table S1). Glove thickness was not hypothesized to influence residue release, as the analyzed residues rest on the glove surface.[1] Samples with the same numeric abbreviation (e.g., L1 and N1) were sourced from the same manufacturer.

product	abbreviation	material	textured portion	finger thickness (mm)
Ansell Nitrilite® 93-401, Silky Ultra-Clean, Gloves	CR	nitrile	finger	0.15
Fisherbrand™ Powder Free Latex Gloves	L1	latex	all	0.16
Kimberly Clark Professional™ Comfort Latex Powder-Free Examination Gloves	L2	latex	finger	0.15
Ansell Microflex™ E-Grip™ Max L92 Latex Gloves	L3	latex	finger	0.16
Fisherbrand™ Powder Free Nitrile Gloves	N1	nitrile	all	0.12
Kimberly-Clark Professional™ Kimtech™ Purple Nitrile™ Gloves	N2	nitrile	finger	0.15
Ansell Microflex™ Supreno™ SE Powder-Free Nitrile Exam Gloves	N3	nitrile	finger	0.18

Table S1. Product, abbreviation, material, textured portion, and finger thickness for all evaluated gloves.

Each glove was imaged using a Leica M125C stereomicroscope equipped with a K5C camera and 2.0X PlanApo objective. The total magnification was 6.4X. As evidenced by the optical images below, particles were visible on the surface of the glove.

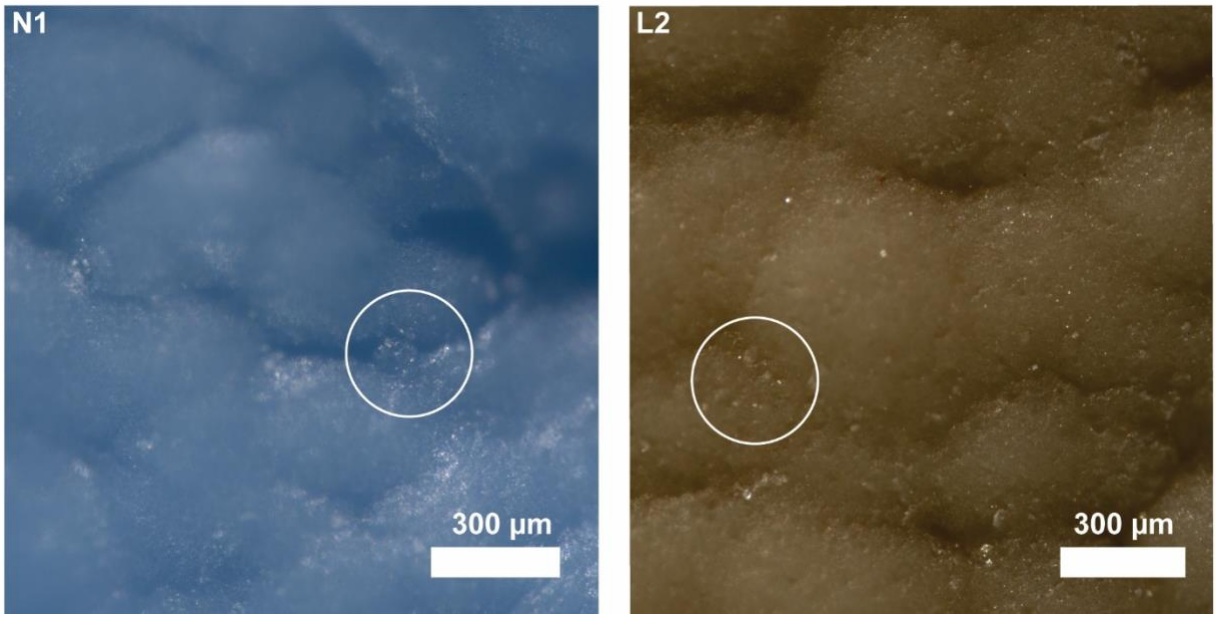

Figure S3. Representative nitrile glove (N1) and latex glove (L2) imaged at 6.4X total magnification. Circles show the locations of particles resting on the glove surface.

III. Investigating dry residue release from laboratory gloves

Preparing laboratory gloves and substrates for contact – In a purged laminar flow hood, an aluminum-coated silicon disc (Angstrom Engineering, QA05-00491, 4-inch diameter, 100 nm thick coating) was scored and cut into small rectangular pieces (~ 1 cm × 1 cm) using a scoring pen and clean metal tweezers in a purged laminar flow hood. The cut substrate was adhered to a stainless-steel microscopy stub using carbon tape and the stubs were housed in individual single-stub storage tubes (Ted Pella, 16630). Next, the textured, index finger portion of each glove sample was cut with scissors, and glass microscope slides were inserted into the glove finger to provide a flat surface in the fingertip portion of the gloves. Labeling tape was used to secure the cut edge of the glove to the microscope slide. The glove-covered microscope slides were then placed in clean, glass petri dishes for storage and transport.

Texture analyzer methodology – In brief, the aluminum-coated silicon substrate was adhered to a stainless-steel probe on the TA×XT-Plus texture analyzer using carbon tape. A glove-covered microscope slide was secured directly under the probe. The instrument was programmed to perform a compression test with a target mode of force. The probe and affixed substrate were lowered to the microscope slide at a constant speed of 0.02 mm/s, exerted a maximum force of

30 N to the surface of the glove-covered microscope slide, and then retracted from contact at a speed of 10 mm/s. Each trial generated a force versus distance curve, displaying the movement of the probe into contact with the slide, its continual compression to the target 30 N force, and the retraction of the probe (Figure S4).

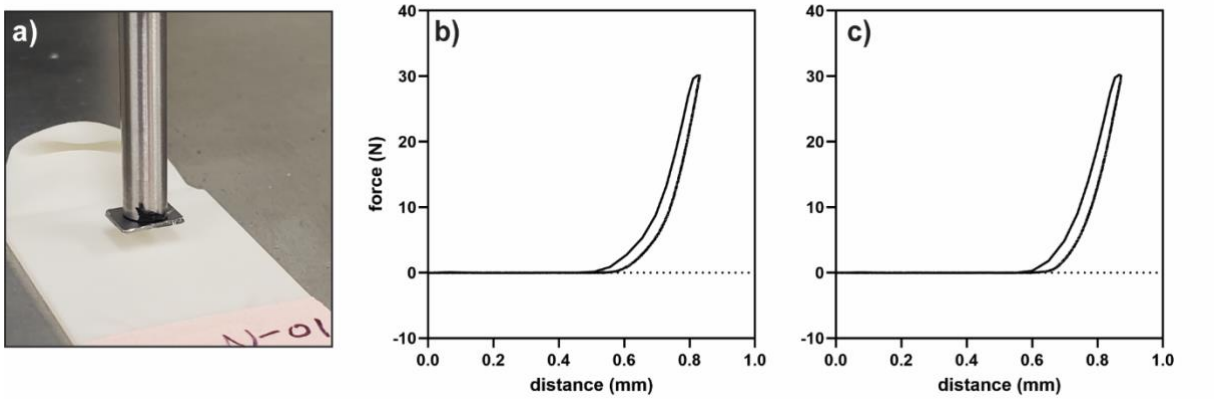

Figure S4. Representative (a) sample collection image, and force versus distance curves for (b) substrate one and (c) substrate two of glove brand L3.

mIRage optical photothermal infrared + Raman methodology – The mIRage optical photothermal infrared (O-PTIR) + Raman spectrometer (Photothermal Spectroscopy Corp.) uses visible (Nikon, CFI S Plan Fluor ELWD 20 × 0.45 numerical aperture, 6.9 mm working distance, 236 × 315 µm field of view) and Cassegrain objectives (Thor Labs, 40 × 0.78 numerical aperture, 8.3 mm working distance, 125 × 166 µm field of view) to respectively visualize and collect simultaneous photothermal infrared (PTIR) and Raman spectra via a pulsed infrared quantum cascade laser (dual-range mIRcat-QT, 120 mW power, 10% duty cycle, 100 kHz pulse rate, 500 nm pulse width) and a 532 nm continuous wave probe laser (200 mW).

mIRage O-PTIR + Raman subsampling – We hypothesized that a random survey of coordinates would best capture particle release differences related to an uneven topology of the textured glove surface. To facilitate spectral collection, the stage coordinates of the corners of each substrate were recorded and used as outer bounds of a random number generator. Ten sets of x,y-stage coordinates were generated for each substrate and, at each location, a 375 × 500 µm mosaic image was collected with the 40X Cassegrain objective. From the collected mosaic images, the featurefindIR® module (PTIR Studios v4.6) determined the coordinates and diameters of imprinted glove residues > 0.5 µm via contrast thresholding for optical particle population statistics. Chemical information via PTIR and Raman spectra were collected from three or four (depending on the quantity of particles in each mosaic) of the ten generated coordinate locations for approximately 100 spectra collected per substrate. All ten collected mosaics were used for optical information. The featurefindIR® module was used to tabulate particle projected area diameter.

mIRage O-PTIR + Raman spectral collection parameters – PTIR spectra were collected using a 100 cm^{-1}/s scan rate at 48% IR power, 5% probe power, a spectral resolution of 2 cm^{-1}, and ten averages of 30 s integrations. PTIR signal was collected from 948–1860 and 2698–3002 cm^{-1} with a 2X detector gain. The Raman spectra were acquired with a grating of 600 grooves/mm and a resolution of 3.4 cm^{-1}, using 5% laser power, a 30 s photobleach delay, and three averages of 30 s integrations. Raman signal was collected from 170–4000 cm^{-1}. A baseline correction was applied in PTIR Studios v4.6 to all Raman spectra prior to export (baseline removal strength: 20).

IV. Creating standard spectral reference libraries

Standard stearate spectral reference library – To create a stearate reference spectral library, standard granule samples of sodium stearate (TCI, >97%), magnesium stearate (Thermo Scientific Chemicals, 3.8–5.0% magnesium), calcium stearate (Spectrum Chemical MFG Corp, NF), and zinc stearate (Aldrich, technical grade) were selected. An aluminum-coated silicon substrate (Angstrom Engineering, QA05-00491, 4-inch diameter, 100 nm thick coating) was scored and cut (~ 1 cm × 1 cm) with a scoring pen and clean metal tweezers in a purged laminar flow hood. Using a clean metal spatula, particles of each chemical identity were sprinkled onto separate aluminum-coated silicon substrates. The substrates were affixed to stainless-steel microscopy stubs with carbon tape and secured in microscopy stub storage tubes before agitation with a Vortex-Genie 2 mixer to dislodge loose particles on the substrate surface.

Using the mIRage O-PTIR + Raman, the featurefindIR® module was used to identify the xy-stage coordinates of ~100 particles > 0.5 µm across multiple fields of views on each substrate for computer-controlled spectral collection. The PTIR spectra were acquired at a 100 cm^{-1} scan rate using 24% IR power, 5% probe power, and ten averages of 30 s integrations. PTIR signal was collected from 948–1860 and 2698–3002 cm^{-1} with a 2X detector gain. The Raman spectra were acquired at a resolution of 3.4 cm^{-1} using 5% laser power, a 30 s photobleach delay, and three averages of 30 s integrations. Raman signal was collected from 170–4000 cm^{-1}.

Spectra were inspected and compared to literature reports of stearate spectra to ensure library quality.[1,2,3] Spectra were included in the standard stearate library where high SNR and agreement with literature peak locations was observed, totaling an average of ~80 PTIR and ~45 Raman spectra per standard. As expected, higher spectral diversity is observed between the PTIR spectra of each standard than the Raman spectra, where no spectral indication of cation identity is observed due to the carboxylate stretch being Raman inactive (Figure S5). All standard stearate spectra used as reference library spectra are available free of charge as supplemental files. It should be noted that high agreement between PTIR and FTIR standard spectra has been established in the literature,[4,6] and therefore the use of these PTIR reference libraries (transformed to transmission) with FTIR test data is expected to effectively predict spectral identity.

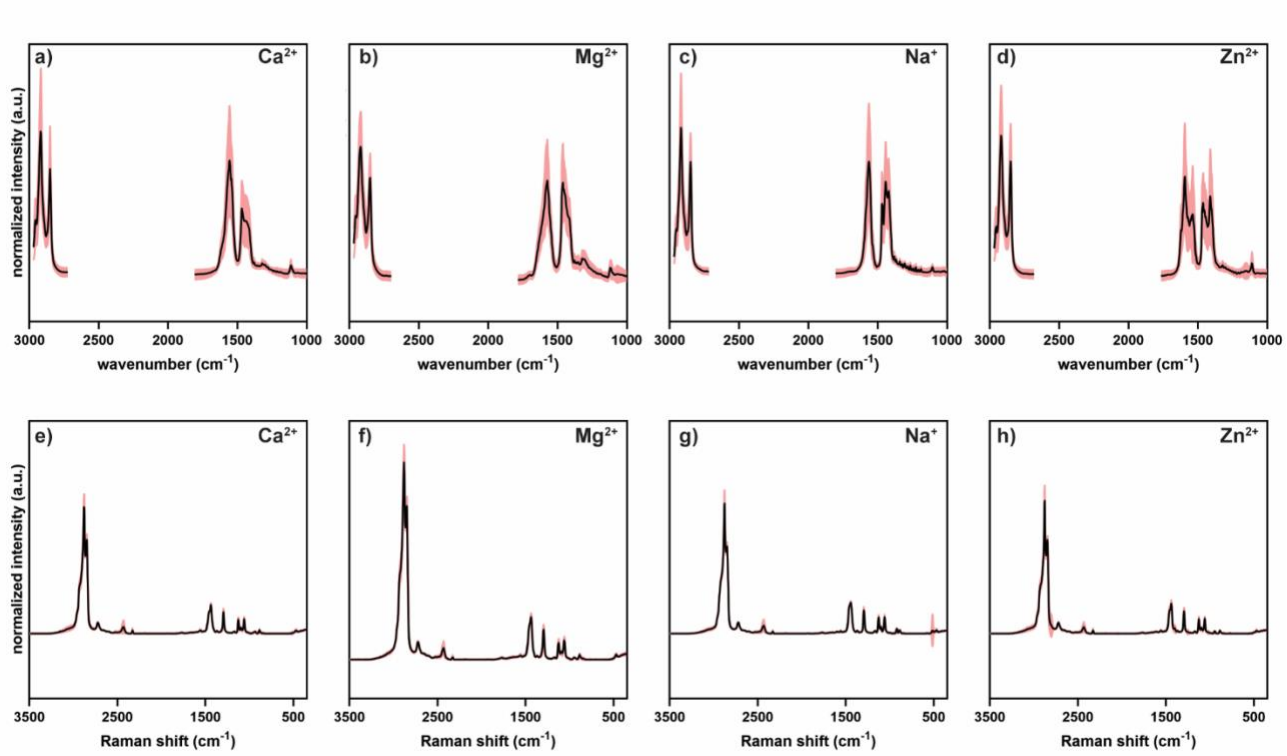

Figure S5. Average normalized PTIR (a–d) and Raman (e–h) spectrum (black) and shaded standard deviation (red) of (a,e) calcium, (b,f) magnesium, (c,g) sodium, and (d,h) zinc stearate standards.

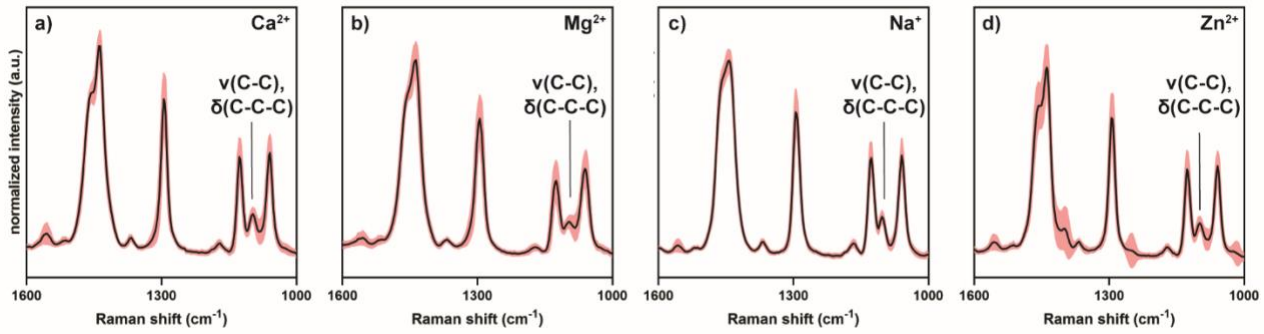

Figure S6. Average normalized Raman spectrum (black) and shaded standard deviation (red) of (a) calcium, (b) magnesium, (c) sodium, and (d) zinc stearate standards between 1000 and 1600 cm^{-1}, showing the location of the distinguishing stearate peak.

Standard microplastic spectral reference library – An additional reference library previously collected using the mIRage O-PTIR + Raman was used for spectral matching to MP standards of polyethylene (Cospheric, high-density PE [HDPE], 0.2–9.9 µm), polypropylene (PP, Nanochemazone, 99% purity, 1–5 µm), and polystyrene suspended as a latex (PS, Polysciences, Inc., 1.75 and 2.5 µm).[5] In brief, each powder was aerosolized with a Collison nebulizer and

impacted onto aluminum-coated silicon substrates. Additional information on the creation of samples for the reference library can be found in the work of Ault and coworkers.[5] Spectra were compared to literature spectra of MP standards to ensure agreement with standard recorded peaks.[6] The reference library was compiled to contain of an average of ~20 PTIR and ~20 Raman spectra per species. The MP spectra were numbered in accordance with the reference library provided by Ault and coworkers,[5] and files detailing which spectra were selected are available as supplemental files.

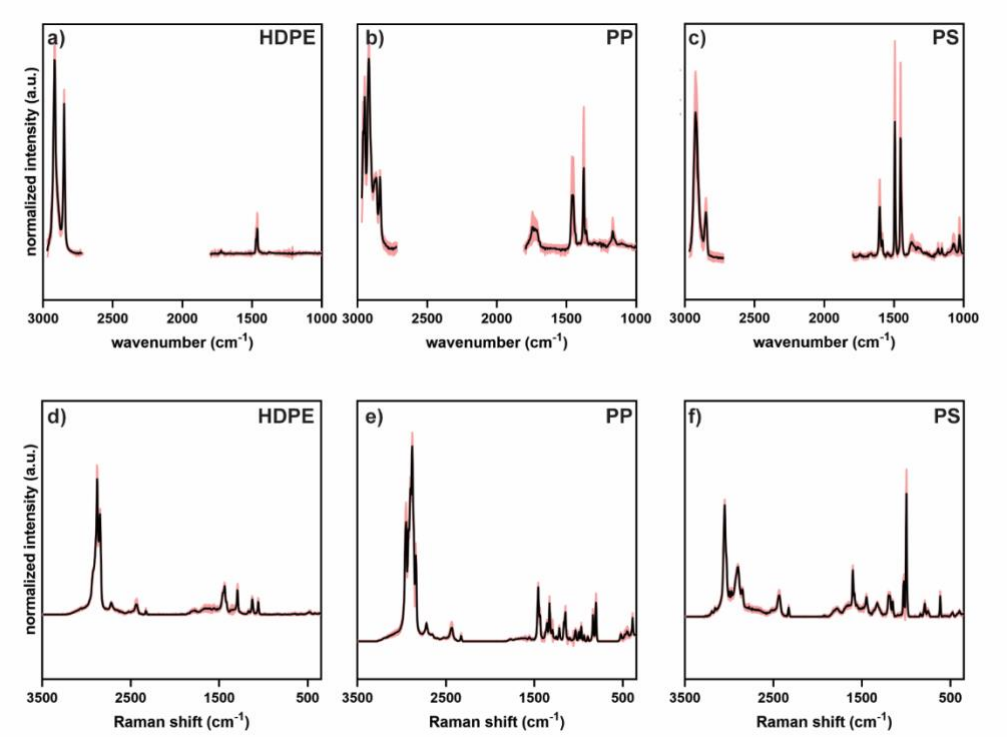

Figure S7. Average normalized PTIR (a–c) and Raman (d–f) spectrum (black) and shaded standard deviation (red) of (a,d) high-density polyethylene (HDPE), (b,e) polypropylene (PP), (c,f) polystyrene (PS) microplastic standards.

V. Preprocessing, excluding, and library matching of acquired spectra

PTIR spectral preprocessing and exclusion – The contents of the PTIR spectral libraries and all residue spectra were first interpolated such that all wavenumbers aligned, which was necessary due to shifting of wavenumber collection ranges on a shared instrument. Then, the PTIR spectra were truncated to the wavenumber ranges of 980–1800 and 2720–2970 cm^{-1} to remove regions of high intensity due to laser chip transitions. Next, all PTIR spectra were normalized using the standard normal variate (SNV) normalization[7] defined as:

$$\bar{X} = \frac{X - \mu}{\sigma} \quad (S1)$$

In equation S1, $\bar{X}$ represents the SNV-normalized spectrum, X represents the spectrum without normalization, μ represents the mean signal of the spectrum, and σ represents the standard deviation of the signal. To limit spectra with a low SNR from influencing the proportion of stearate library matches observed from glove contact, we employed an exclusion rule based on the total variation (TV) of the unidentified spectrum compared to a distribution of total variation from manually labeled low SNR spectra from each glove brand in the residue particle dataset. Total variation, described in equation S2, is a metric that measures how much a function (the spectrum) oscillates or fluctuates.[8] A high total variation suggests rapid fluctuations or sharp peaks in the spectrum, which we used as a proxy to indicate spectral noise.

$$TV(f) = \sum_{w} |f(w+1) - f(w)| \tag{S2}$$

In equation S2, *TV(f)* refers to the total variation of the function and *w* refers to wavenumber. For our use, we calculated the total variation of PTIR signal intensity in three sections (980–1170 cm^{-1}, 1290–1800 cm^{-1}, and 2720–2980 cm^{-1}) to avoid noise from laser chip transitions (Figure S8).

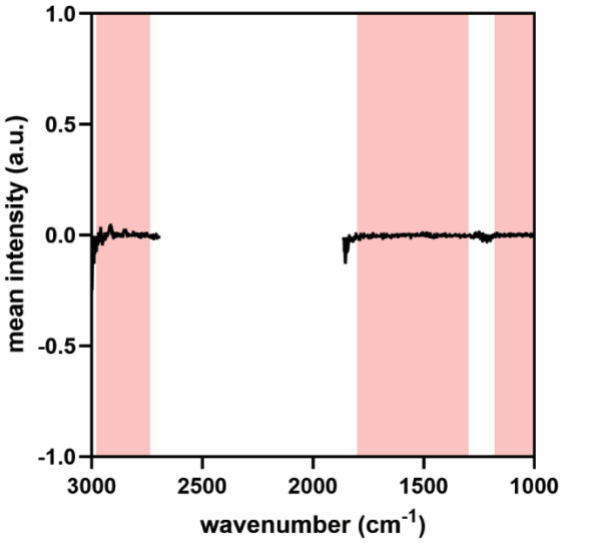

Figure S8. Exemplative low signal-to-noise ratio PTIR spectrum (black) with highlighted regions (red) to illustrate where total variation was calculated, avoiding noisy chip transitions and regions where no signal is recorded.

To build a distribution of total variation from manually labeled low SNR spectra, 20 examples of low SNR spectra were selected from each glove brand (Figure S9). Figure S10 reflects the total variation distribution of the selected spectra. We chose to use the 1% quantile on the labeled total variation distribution of low SNR spectra as a threshold for determining which glove-residue spectra were statistically distinguishable from low SNR spectra. This choice of threshold coincides

with a typical 3σ SNR rule on a normal distribution, where the false positive rate (proportion of spectra with high SNR excluded from spectral matching) was fixed at 1%.[9] To validate this false negative rate, we next subjected 20 manually labeled high SNR spectra from each glove brand to the total variation exclusion rule and found that the exclusion rule leads to a false positive rate below 1% and a false negative (spectra with low SNR included in spectral matching) rate of ~ 2%. On average, this exclusion rule reduced the PTIR residue data per glove brand by 18% (Figure S11), removing low SNR spectra from the matching pipeline (Figure S12).

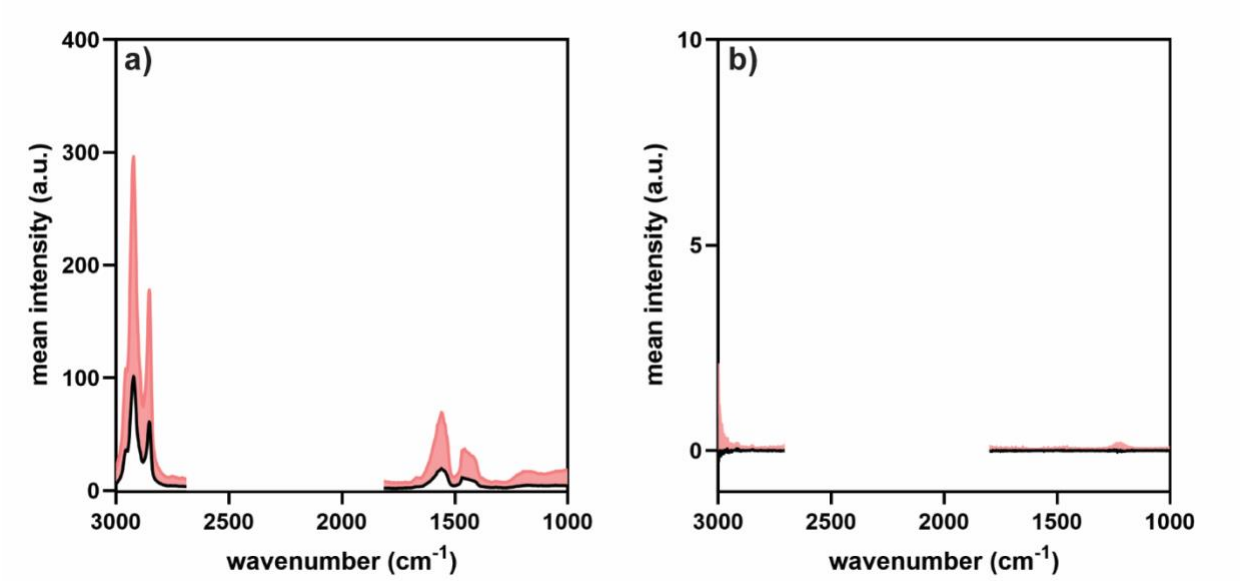

Figure S9. Average (black) and shaded positive standard deviation (red) of manually labeled (a) high and (b) low signal-to-noise ratio PTIR spectra accumulated from 20 manually labeled spectra per glove brand.

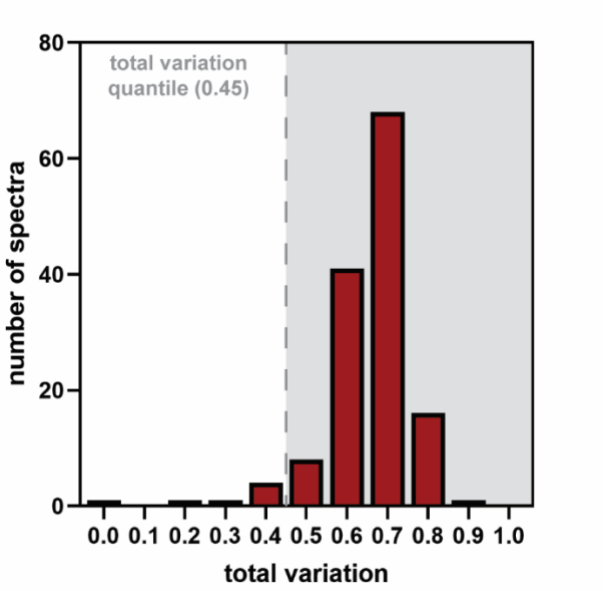

Figure S10. Distribution of total variation built from manually labeled low signal-to-noise ratio spectra. The 1% quantile is shown as a dashed line at x = 0.45, indicating that the total variation is lower than 99% of the data (shaded in gray).

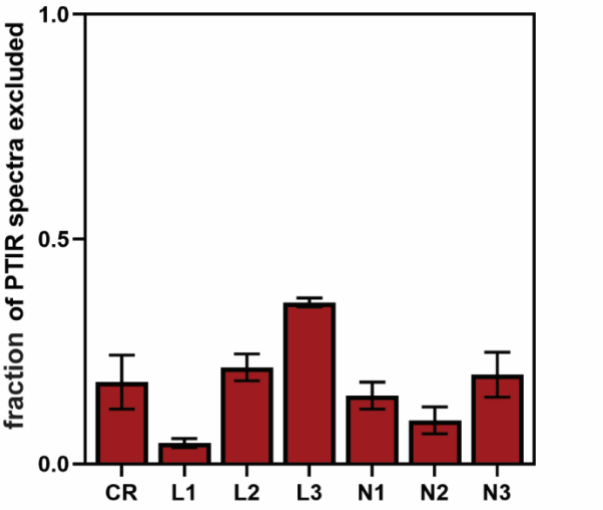

Figure S11. Fraction of all collected PTIR spectra removed by the total variation exclusion rule from each glove brand.

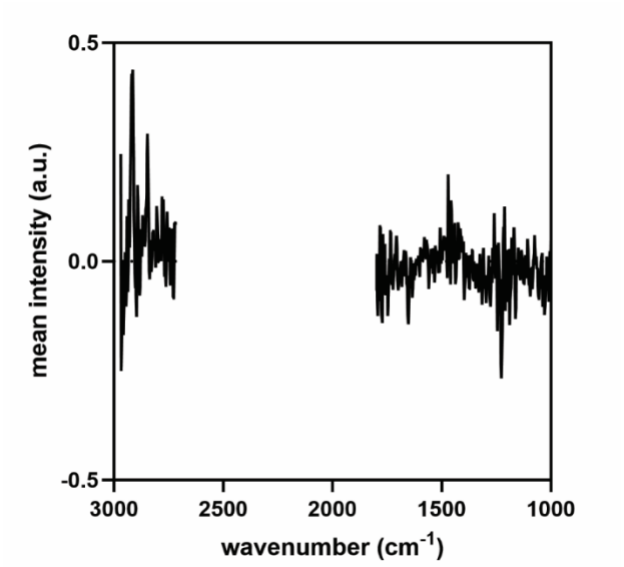

Figure S12. Average normalized PTIR spectra removed from matching pipeline due to institution of the total variation exclusion rule.

Raman spectral preprocessing and exclusion – All non-volatile residue and library Raman spectra collected using the mIRage system were preprocessed by first interpolating all wavenumbers to align. This step was necessary due to a shift in wavenumber range relating to the need to manually calibrate the Raman spectra to a silicon standard. The spectra were then truncated to a wavenumber range of 355–3500 cm^{-1} to reduce high intensity values at the extreme wavenumbers, which would influence automated spectral matching. Next, spectra with saturation present (i.e., intensity values reached the maximum detection limit) were removed to avoid interference with library matching practices.

On average, the exclusion of saturated spectra removed 16% of Raman spectra per glove brand (Figure S13). The Raman spectra removed due to saturation were most commonly found to be saturated at 520 cm^{-1}, indicating that surface defects in the aluminum-coated silicon substrate may have been mistaken for particles by the featurefindIR® module, leading to Raman spectra of silicon background signal (Figure S14). The remaining spectra were then baseline corrected via the Specy correction and normalized using the standard normal variate normalization.[10,11] The Raman spectra were then calibrated to the ambient N_2 peak at 2330 cm^{-1}.[5,12]

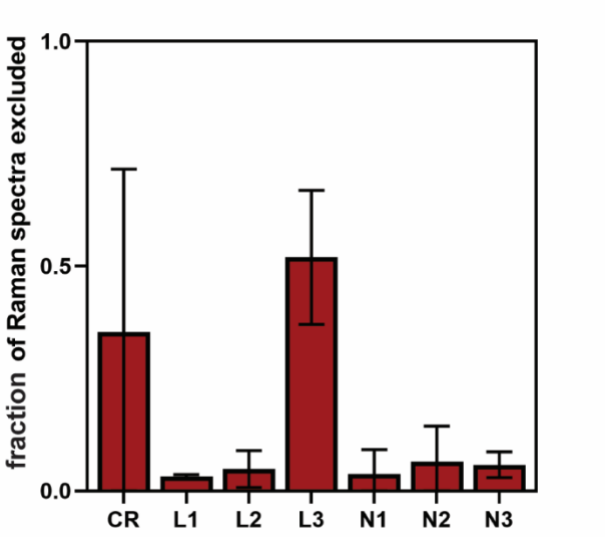

Figure S13. Fraction of all collected Raman spectra removed by the saturation exclusion rule from each glove brand. Note that error bars represent standard deviation.

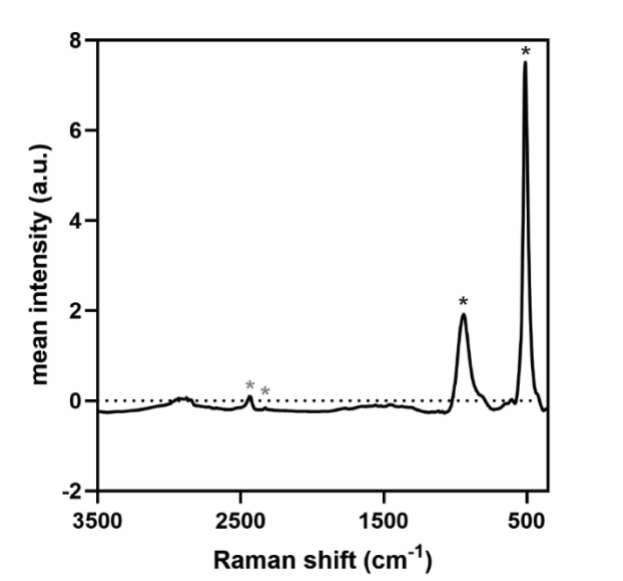

Figure S14. Average normalized Raman spectra removed from matching pipeline due to institution of the saturation exclusion rule. Black asterisks indicate peaks attributed to the substrate surface (silicon underneath a layer of aluminum) and gray asterisks indicate spectral artefacts not related to the particle (ambient nitrogen and fluorescent lamp).

Spectral matching with Pearson correlation coefficient – Pearson correlation coefficient (PCC) is described by equation S3. Denoting x_{test} and x_{ref} as the spectral vectors containing the normalized intensities at each wavenumber, we express *PCC* as:

$$PCC = \frac{\mathrm{cov}(x_{test}, x_{ref})}{\sigma_{test}\sigma_{ref}} \quad (S3)$$

Where $\mathrm{cov}(x_{test}, x_{ref})$ is the covariance between spectra x_{test} *and* x_{ref}, and $\sigma_{test}, \sigma_{ref}$ represent the standard deviations of x_{test} and x_{ref}, respectively.

We chose PCC as the matching algorithm and 0.7 as the HQI threshold to illustrate the potential for MP false positives using the most common automated spectral matching routines in the literature.[13]

VI. Visualizing particle morphology with scanning electron microscopy

Visualizing glove residues – The glove species with the highest observed MP false positive rate (L1) was selected to obtain morphological information of glove-imprinted particles via scanning electron microscopy (SEM). The sample was prepared and obtained using the same process as all other samples, except that the substrate used was gridded silicon (Rave Scientific) rather than aluminum-coated silicon. A gridded substrate was necessary to correlate chemical signal from the mIRage system to optical information obtained via SEM. After repeating the texture analyzer methodology outlined in Section III, the gridded silicon substrate was analyzed with the mIRage system to confirm stearate presence in one grid (1 x 1 mm) of the substrate (Figure S15). The substrate was next sputter coated with gold for 80 s using a SPI-Module Carbon/Sputter Coater. The same grid that was chemically analyzed was visualized at tilt conditions of 0°, 45°, and 90° using a Tescan MIRA3 FEG instrument (14.5 kV accelerating voltage, beam intensity 8) with an Everhart-Thornely image detector to observe particle size, morphology, and thickness. Representative images of non-volatile residues from glove contact are presented in Figure S16.

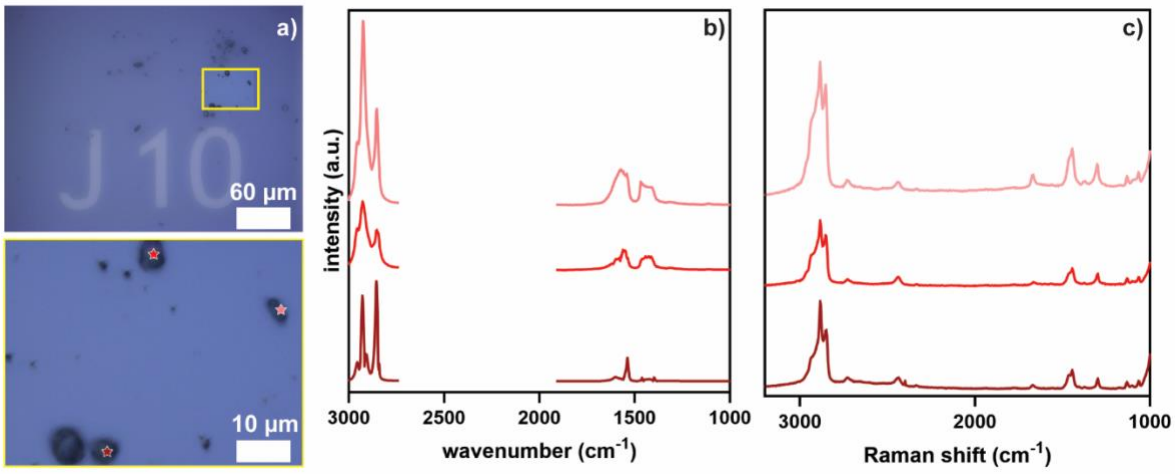

Figure S15. mIRage O-PTIR + Raman analysis of gridded silicon substrate post-dry contact (30 N) with an L1 glove, including (a) optical images of grid location, where the bottom image shows the spectral collection field of view, (b) PTIR spectra, and (c) Raman spectra correlated to the optical image via color-coded stars.

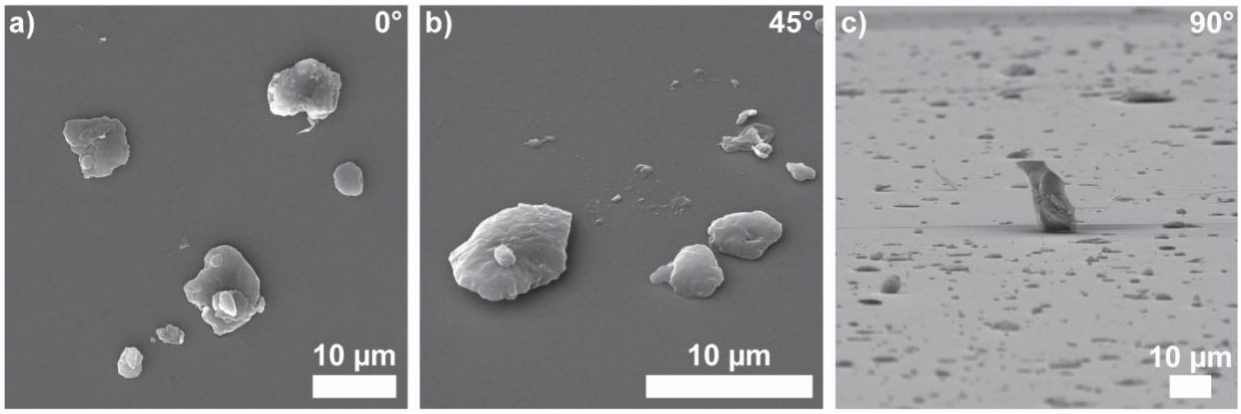

Figure S16. Representative images of non-volatile residues released from dry contact with laboratory gloves via scanning electron microscopy with (a) 0° tilt, (b) 45° tilt, and (c) 90° tilt.

Visualizing polyethylene particles – A rotary tool equipped with a diamond burr tip was used to mechanically break down the surface of a post-consumer HDPE sample. The microplastics generated were then gently pressed onto a gridded silicon substrate with tweezers to transfer the particulate matter for analysis via the mIRage system. The gridded silicon substrate was analyzed with the mIRage system to confirm HDPE presence and note where the particles were observed for targeted SEM analysis (Figure S17). The substrate was next sputter coated with gold for 80 s using a SPI-Module Carbon/Sputter Coater. The same grid that was chemically analyzed was visualized at tilt conditions of 0° and 45° using a Tescan MIRA3 FEG instrument (14.5 kV accelerating voltage, beam intensity 8) with an Everhart-Thornely image detector to observe particle size, morphology, and thickness. For this sample, 90° tilt conditions were not collected due to concerns that particles may move from their known location. Representative images of post-consumer HDPE particles are presented in Figure S18.

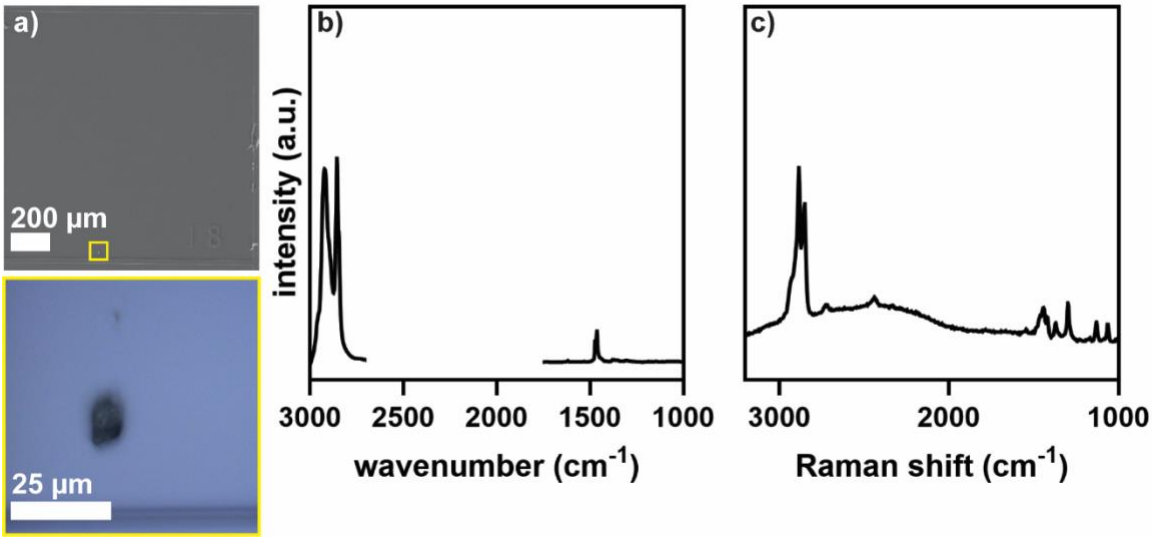

Figure S17. mIRage O-PTIR + Raman analysis of gridded silicon substrate post-generation of polyethylene microplastics, including (a) electron (top) and optical (bottom) images of grid location, where the bottom image shows the spectral collection field of view, (b) PTIR spectra, and (c) Raman spectra of the analyzed particle.

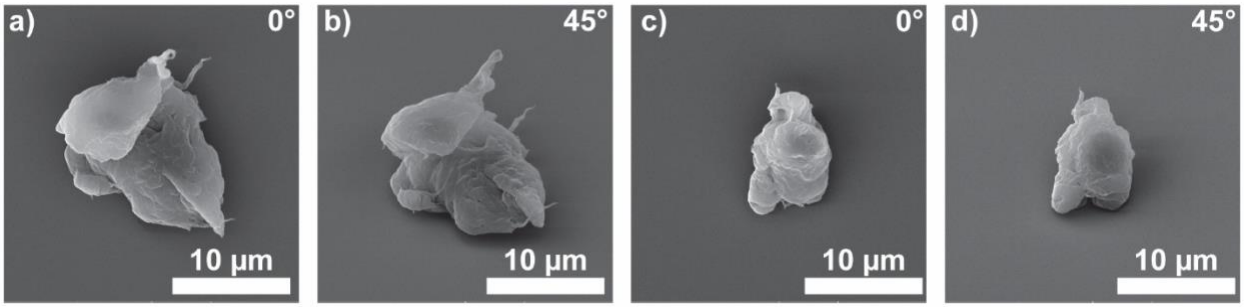

Figure S18. Additional images of O-PTIR + Raman confirmed polyethylene particles via scanning electron microscopy with (a) 0° tilt, (b) 45° tilt of the same particle, and (c) 0° tilt, (d) 45° tilt of the same particle.

VII. Investigating potential for false positives in Fourier transform infrared spectroscopy

Texture analyzer methodology – Additional aluminum-coated silicon substrates and glove-covered glass microscopy slides of a single latex glove type (L1) were prepared as previously described. The same methodology previously used for sample collection with the TA×XT-Plus texture analyzer was used for the preparation of substrates with greater applied contact forces. The only change to the methodology described in Section III was the programmed maximum force, which was changed to 60 N, 90 N, and 120 N for the collection of two aluminum-coated substrates that came into dry contact with a new glove (L1) per applied force. Exemplative force versus distance curves for this experiment are shown in Figure S19.

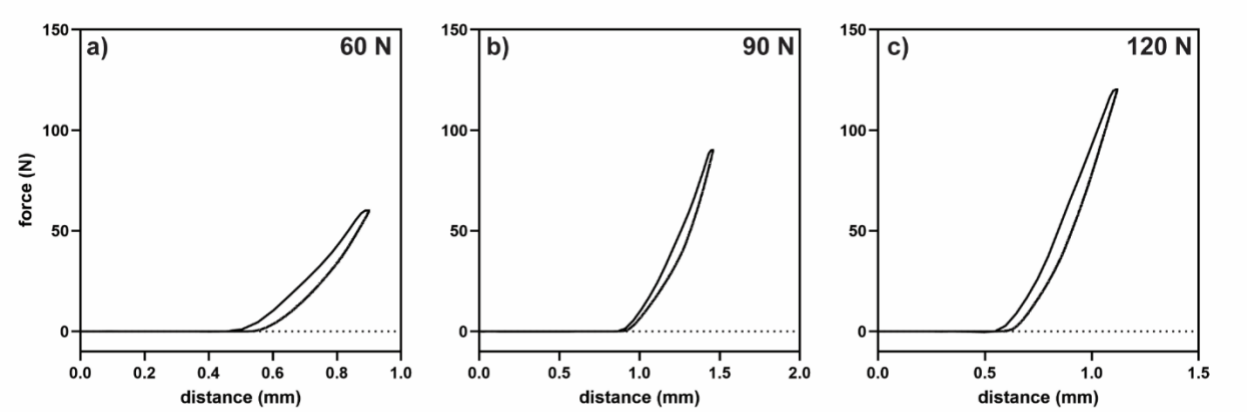

Figure S19. Representative force versus distance curves for (a) 60 N, (b) 90 N, and (c) 120 N applied force between glove L1 and the substrate.

mIRage optical collection and ImageJ methodology – Using the mIRage system, ten sets of x,y-stage coordinates were randomly generated for each substrate and a 375 × 500 μm mosaic image was collected with the 40X Cassegrain objective at each coordinate. Due to observing a high occurrence of particle overlap (Figure S20), rather than quantify the size of discrete particles using the featurefindIR® as in the 30 N samples, ImageJ was used to quantify surface area coverage. An ImageJ macro was created to binarize and threshold (Phansalkar localizing algorithm, radius 100) all mosaic images from the 30, 60, 90, and 120 N duplicate substrates for a single latex glove brand (L1), such an average surface area fraction measurement was obtained for each contact force. Although the sizes of residues from dry contact with gloves are smaller than observed from wet gloves, higher contact forces applied between the glove and the metal substrate led to higher non-volatile residue surface coverage (Figure S21).

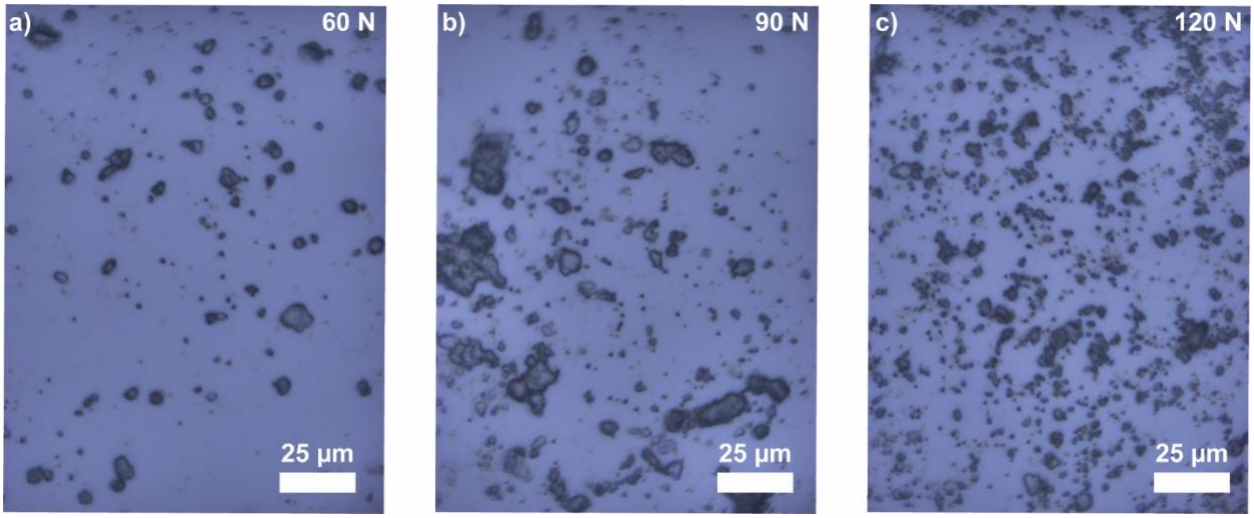

Figure S20. Representative images from the mIRage system of aluminum-coated substrate after (a) 60 N, (b) 90 N, and (c) 120 N applied contact force with L1 glove samples.

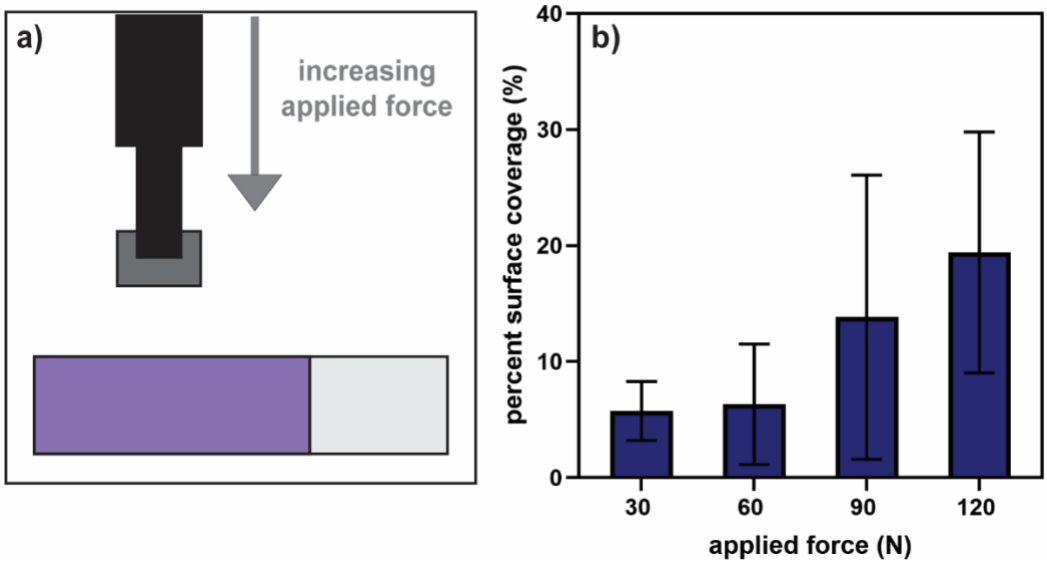

Figure S21. Depiction of (a) workflow to obtain samples with higher glove contact forces, and (b) the percent surface area coverage of non-volatile residues on the substrate with increasing applied forces. Note that error bars represent standard deviation.

Fourier transform infrared (FTIR) spectroscopy – To investigate whether the agglomeration of these small particles influence more traditional transmission FTIR measurements, which are often limited to particles > 10 µm,[14] we made dry contact between a gloved (L1) hand and an aluminum-oxide filter (Whatman Anodisc, 47 mm, 0.2 µm pore size), commonly used in MP research.[14,15] The cooled detector of a Nicolet iN10 Infrared Microscope (Thermo Scientific) was used to evaluate the surface of an aluminum-oxide filter (Whatman) that was touched by a researcher's

gloved (L1) fingertips. Signal was collected from 1350–4000 cm^{-1} with a 15 × 15 µm aperture and 32 scans at 4 cm^{-1} resolution. A background spectrum of an unused aluminum-oxide filter was auto-subtracted from each sample spectrum. The resultant µFTIR spectrum indicates that stearate surface coverage from dry contact influences more than just the single-particle measurements investigated herein, as clear peaks attributed to stearate species are observed in the spectrum collected from a film-like covering of glove-released particles (Figure S22).

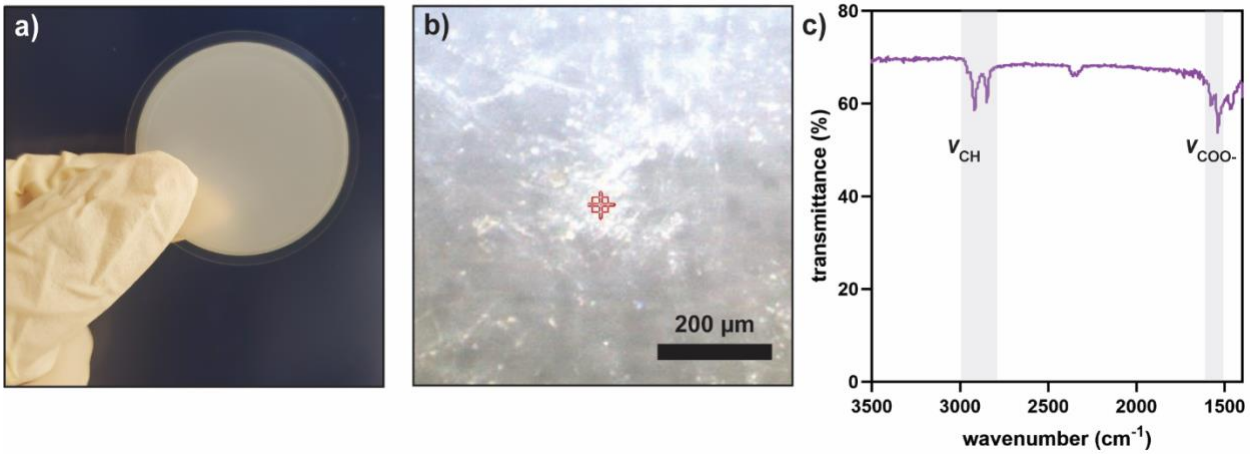

Figure S22. Depiction of (a) dry glove contact with an aluminum-oxide filter, (b) optical image of aluminum-oxide filter surface with white, shiny, glove-imparted film coating, and (c) plot of average µFTIR measurements of film, with major spectral contributions from stearates labeled.

Modified, automated analysis of µFTIR spectra – Using the pipeline established in the main text, we evaluated if the µFTIR spectrum in Figure S22 could be differentiated from HDPE examples. When truncated to the suggested extended fingerprint range (here, 1350–1800 cm^{-1}), transformed from transmission to reflection according to the Beer-Lambert law, where %T is percent transmittance and A is absorbance (equation S4),[24] and matched to the combined PTIR stearate and MP library, a higher HQI is attributed to a stearate match (HQI = 0.85, zinc stearate) than an MP match (HQI = 0.31, HDPE). This result indicates that FTIR spectra of stearate contaminants can be successfully differentiated from MPs using the pipeline established in the main text for PTIR spectra.

$$\mathrm{A} = 2 - \log_{10}(\%T) \tag{S4}$$

Investigating automated analysis of weathered FTIR spectra – The weathering of environmental PE can lead to an increase in the carbonyl index of the spectrum.[16] Although the carbonyl peak is distinct between weathered PE and stearate examples in PTIR, occurring between 1680–1800 cm^{-1} and 1550–1580cm^{-1}, respectively,[2,16,17,26] we wanted to understand the suitability of our outlined PTIR differentiation pipeline to weathered µFTIR measurements. We selected a weathered PE example (PE #38) from the "FTIR library of plastic particles sourced from the

environment (FLOPP-e)"[23] library due to its clear carbonyl peak (Figure S23). Following our suggested pipeline in the main text, we truncated the data to the extended fingerprint range (980-1800cm^{-1}), and matched the spectrum to the combined PTIR stearate and MP library. We found that a higher HQI was attributed to an HDPE example (HQI = 0.78) than a stearate example (HQI = 0.54), illustrating that weathered PE spectra can likewise be differentiated using our proposed workflow.

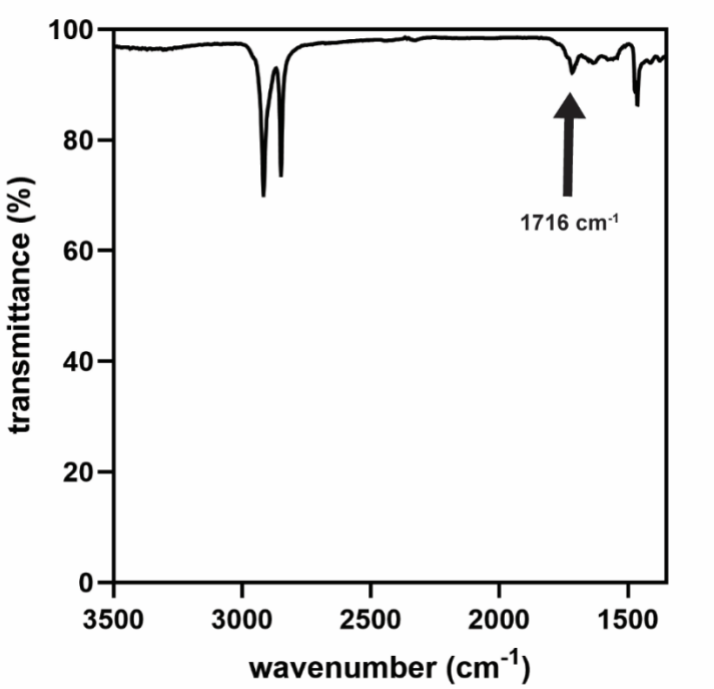

Figure S23. Polyethylene example #38 from the "FTIR library of plastic particles sourced from the environment (FLOPP-e)" with the location of the carbonyl peak labeled.

VIII. Conformal prediction methodology

Conformal prediction theory – Conformal prediction (CP) is a statistical method that, when applied to vibrational spectroscopy data, allows a user to obtain predictions of spectral identities with a theoretical guaranteed confidence, or probability, of encountering the correct identity in the set of predictions.[18,19] CP uses a calibration dataset to represent the expected variability of unidentified spectra, allowing new spectra to be labeled with a theoretical guaranteed confidence. Mathematically, let us consider a similarity metric calculated for a new spectrum x and for each chemical identity in the reference library denoted by $\left(\hat{f}(x)_1, \ldots, \hat{f}(x)_K\right)$. We define the score $s_i = 1 - \hat{f}(X_i)_{Y_i}$ as the HQI of example i corresponding to its known identity. For our calibration set, we next introduce independent and identically distributed data points, denoted as $(X_1, Y_1), \ldots, (X_n, Y_n)$, where X represent the spectral data and Y represent the true chemical identity. For an unknown spectrum that we wish to identify, represented as X_{test}, and given a desired

theoretical confidence guarantee of $1-\alpha$, we can construct a prediction set defined as $\mathcal{C}_\alpha(X_{\text{test}}) = \{ y\colon \hat{f}(X_i)_y \geq 1 - \hat{q} \}$ where $\hat{q}$ is the $\lceil (n+1)(1-\alpha) \rceil / n$ empirical quantile of the scores $s_1, \ldots, s_n$. The prediction set has the following theoretical confidence guarantee (equation S5):

$$1 - \alpha \leq P[Y_{\text{test}} \in \mathcal{C}_\alpha(X_{\text{test}})] \leq 1 - \alpha + \frac{1}{n+1} \tag{S5}$$

In this work we employed a similarity metric, defined in equation S6, commonly used in the conformal prediction literature known as nearest neighbor (NN).[20]

$$\hat{f}(x)_y = \widetilde{NN}_y = exp\left(-\frac{\min\limits_{ref}\{|x - x_{ref}|\colon y_{ref} = y\}}{\min\limits_{ref}\{|x - x_{ref}|\colon y_{ref} \neq y\}} \right) \tag{S6}$$

NN represents the minimum distance between x and every reference spectra x_{ref} corresponding to the label $y_{ref} = y$ divided by the minimum distance between x and every reference spectra x_{ref} that does not correspond to the label $y_{ref} \neq y$.

NN behaves differently than PCC, but use of the SNV normalization enables the predicted classification labels of NN and PCC to be the same. In brief, NN is a more efficient metric than PCC, allowing it to better distinguish between similar chemical identities.[13] As shown in Figure S24, PCC relies on the absolute relationship between the cosine of the angle between a reference and unknown spectrum. On the other hand, NN relies on the relative distances between the unknown spectrum and various reference spectra. To obtain a high HQI value using NN, it is not enough thata the two spectra are close, it is also necessary that there is no other reference spectrum that is also close. PCC, on the other hand, returns high HQI scores for any nearby reference spectrum.

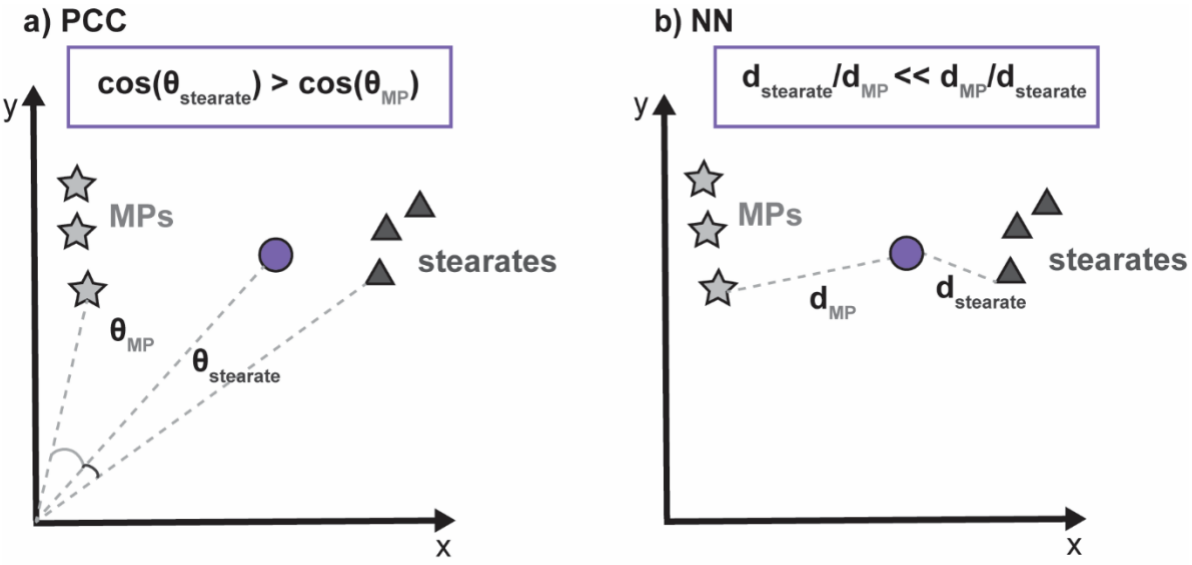

Figure S24. Two-dimensional representation of (a) Pearson correlation coefficient (PCC) and (b) nearest neighbor (NN) metrics, where the purple circle indicates a spectrum of a glove residue, stars represent microplastic (MP) reference spectra, and triangles represent stearate reference spectra. Here, d refers to distance in vector space between the spectra.

The most important assumption in CP revolves around the exchangeability of the calibration set. This exchangeability provides the connection between the theoretical and empirical confidence guarantee. The calibration data points need to be collected independently and represent the expected variability in the unknown spectral data. However, the performance of the similarity metric is also measured by the size of the prediction sets. In short, when two similarity scores return prediction sets with a different number of predicted identities for the same unknown spectrum, the metric that returns the fewest identities with the same confidence guarantee is considered more efficient, as it reduces the manual inspection required to distinguish between predicted identities. It has been shown that NN outperforms other similarity metrics widely used in the literature, like Pearson correlation coefficient. It is important to mention that the size of the prediction set is influenced by how different factors relate to uncertainty: the quality of reference library and similarity metric, the chosen confidence level (higher confidence will lead to larger prediction sets), and the quality of the spectral data that is being analyzed (poor quality spectra will lead to larger prediction sets). It should also be noted that CP cannot predict identities that do not exist in the employed reference library.

One appealing property of CP is that the size of the prediction sets can be used to measure the uncertainty of the matching process. When we employ a matching process like HQI, we can assess how “sure” we are about the chemical identity based in the number of labels in the prediction set returned by CP. The ideal case of CP is when the prediction set only consists of a single label. On the other hand, having many labels in the prediction set indicates higher uncertainty and the need to manually evaluate the chemical identity.

Conformal prediction experimental design – For the results herein, CP was used for the residue Raman spectra from dry glove contact with 30 N force (Scheme S1). We employed a user-defined theoretical confidence guarantee of 95%, generating non-arbitrary HQI thresholds to be met or exceeded for population in the prediction set. To create the Raman calibration set, 50% of the selected stearate reference library, stratified by label, was used in combination with the unsorted (i.e., not selected for reference library), preprocessed stearate spectra. For this application, all spectra collected from the stearate standards were used rather than restricting the calibration set to include only the best reference examples. The inclusion of lower quality spectra from stearate standards than what was used for the reference library better mimics the data quality anticipated in the test set (i.e., unidentified residue spectra), allowing CP to better predict spectral identity. Only residue particle data that matched to a stearate reference spectrum with HQI ≥ 0.7 via non-CP methods were used as test spectra to best evaluate how CP may aid identification of stearate species from gloves. Both the stearate and mIRage MP libraries were used as the reference spectra. For each test spectrum, the contents of the prediction set were analyzed for the number of predicted identities and whether those identities included only MP labels, only stearate labels, both MP and stearate labels, or no labels. The CP methods were repeated with random stratified splits of calibration and reference spectra 500 times such that mean quantities of HQI threshold and number of predicted identities were produced.

Scheme S1. Graphic illustrating the use of conformal prediction with Raman spectra, where exemplative labels relating to the identities of polyethylene (PE) and a stearate species are tracked onto the distribution of hit quality index (HQI) between the calibration set and reference libraries.

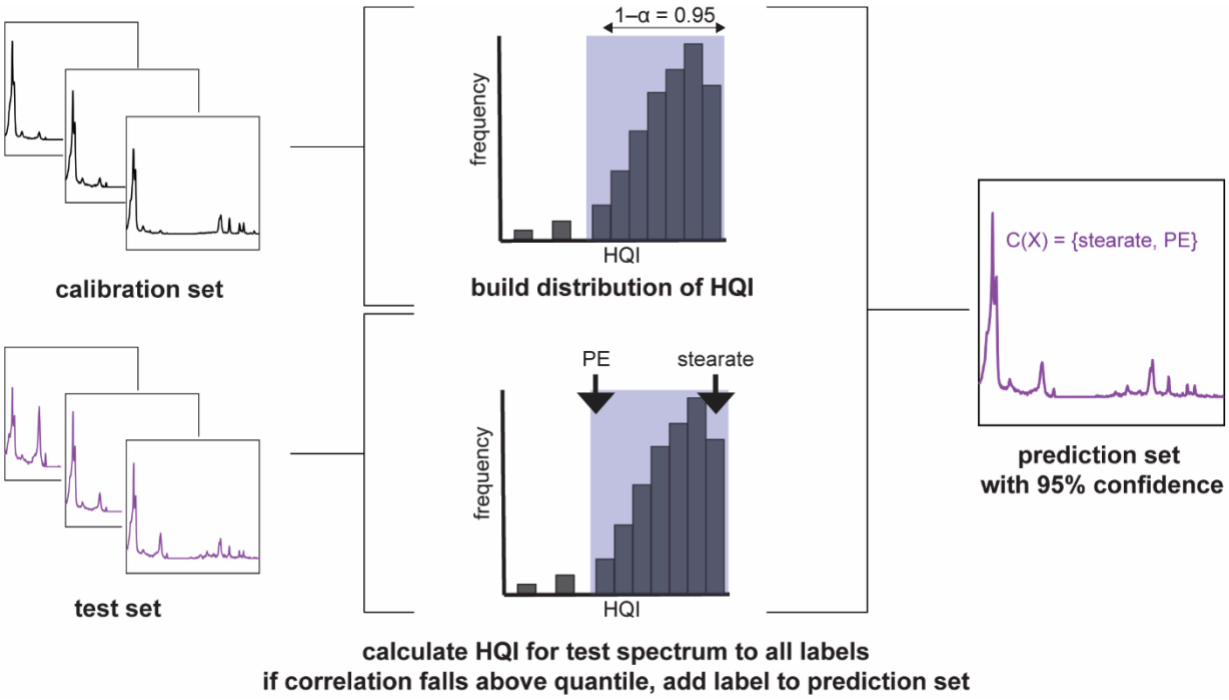

IX. Application to glove-contaminated environmental dataset

Sampling and analysis conditions of environmental dataset – While wearing a 100% cotton laboratory coat, aluminum-coated silicon substrates were prepared as described in Section III, but here nitrile gloves (type N3) were worn as substrates were prepared, and the gloves encountered the surface of the substrates. Cut substrates were housed in individual single-stub storage tubes (Ted Pella, 16630).

Four counties near the University of Michigan were selected to compare the regional quantities and identities of atmospheric microplastics in spring of 2023 (Figure S25). With the aid of community partners at local schools, passive air samplers and housing shelters designed specifically for dry particulate matter deposition[21] were deployed in outdoor parking lot locations of Daycroft School in Ann Arbor, Washtenaw County, Fowlerville High School in Fowlerville, Livingston County, International Academy Okma in Bloomfield Hills, Oakland County, and Intercity Baptist High School in Allen Park, Wayne County. The location of each sampler was chosen to maximize nearby foot and vehicle traffic for MP deposition yet minimize campus disruption (Figure S25). The housing shelters were ratchet strapped to support poles at a height of 5 feet, and three aluminum coated silicon substrates on SEM stubs were transferred with tweezers to the inside of the shelter before the top was replaced (Figure S26). A procedural blank of aluminum coated

silicon was subjected to the same conditions but was immediately removed from the shelter after being placed inside and was then transferred back to the lab for analysis. After the month-long sampling duration (Table S2), the substrates were removed from the shelter with tweezers, placed in capped storage tubes, and transferred back to the laboratory. A 100% cotton laboratory coat and nitrile gloves (type N3) were worn in the field when samples were exposed to air.

As in the subsampling scheme described for the 30 N glove contact samples, a random survey of coordinates was used to determine three locations for chemical analysis on two unique substrates (side-by-side on the sampler) from each collection site. The stage coordinates of the corners of each substrate were recorded and used as outer bounds of a random number generator, and at each location, a 665 × 500 μm mosaic image was collected with the 40X Cassegrain objective. Simultaneous chemical information via PTIR and Raman spectra were collected from approximately 100 particles using the same collection parameters as in Section III. This yielded approximately 200 PTIR and Raman spectra from two substrates at each location, and the chemically analyzed area represented ~1% of total substrate area, on average.

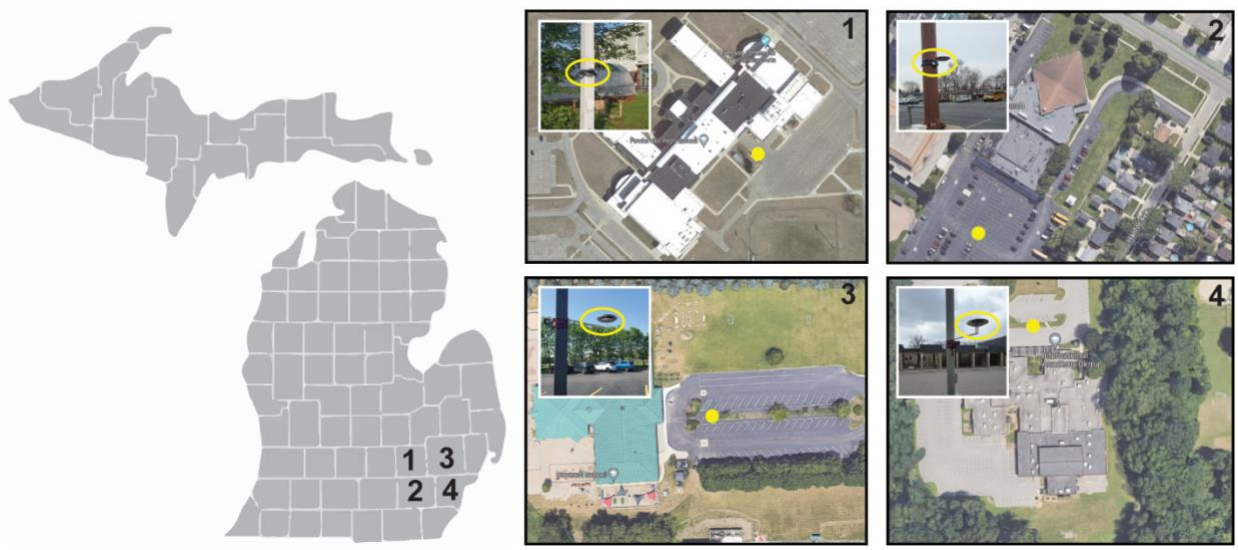

Figure S25. Selected counties, campus images with sampler locations marked by yellow dots, and inset images of deployed housing shelters on site. Here, 1 is Livingston County, 2 is Washtenaw County, 3 is Oakland County, and 4 is Wayne County. Arial images courtesy of Google Maps.

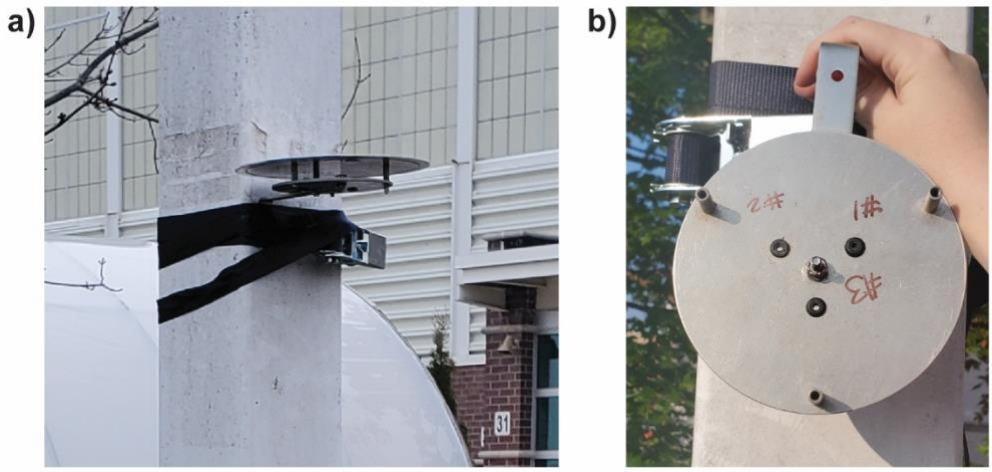

Figure S26. Images from the field of (a) passive sampling housing shelter with protective top for precipitation coverage and (b) passive sampling housing shelter with top removed, where substrates mounted on scanning electron microscopy stubs are placed.

county	school	sampling dates	duration (d)
Washtenaw	Daycroft School	05/10/2023 – 06/07/2023	28
Livingston	Fowlerville High School	05/10/2023 – 06/07/2023	28
Oakland	International Academy Okma	04/26/2023 – 05/25/2023	29
Wayne	Intercity Baptist High School	04/26/2023 – 05/25/2023	29

Table S2. County, school, sampling dates, and duration of sample collection for environmental data analyzed herein.

Manual identification of PTIR and Raman environmental spectra – Prior to manual and automated predictions, all the environmental spectra were preprocessed in the same manner as described in Section V. We used the mIRage MP library to index PTIR and Raman matches (HQI ≥ 0.7) to HDPE, giving 38 PTIR matches, and 110 Raman matches from a total dataset of 2,653 PTIR and Raman spectra. Each spectrum was plotted against the average mIRage calcium stearate and HDPE library spectra and evaluated for similarity to the references such that an “HDPE”, “stearate”, or “uncertain” identity was manually assigned. For the PTIR spectra, fingerprint vibrations attributed to the carboxylate functionality in stearate salts were used to distinguish identities. For the Raman spectra, the distinguishing peaks around 1416 cm^{-1} and 1106 cm^{-1} (as seen in main text Figure 6) were selected for manual distinction between identities. The presence or lack of the peak at 1106 cm^{-1} was used as a consistent diagnostic, as the PE-specific peak at 1416 cm^{-1} is dependent on polymer crystallinity. Spectra where a distinction could not be made (e.g., due to low SNR or fluorescence, or when neither identity matched) were labeled “uncertain” and removed from further analysis as automated results hinge on the quality of input data (Figure S27). Example spectra manually assigned each label are illustrated in Figures S27, S28, and S29.

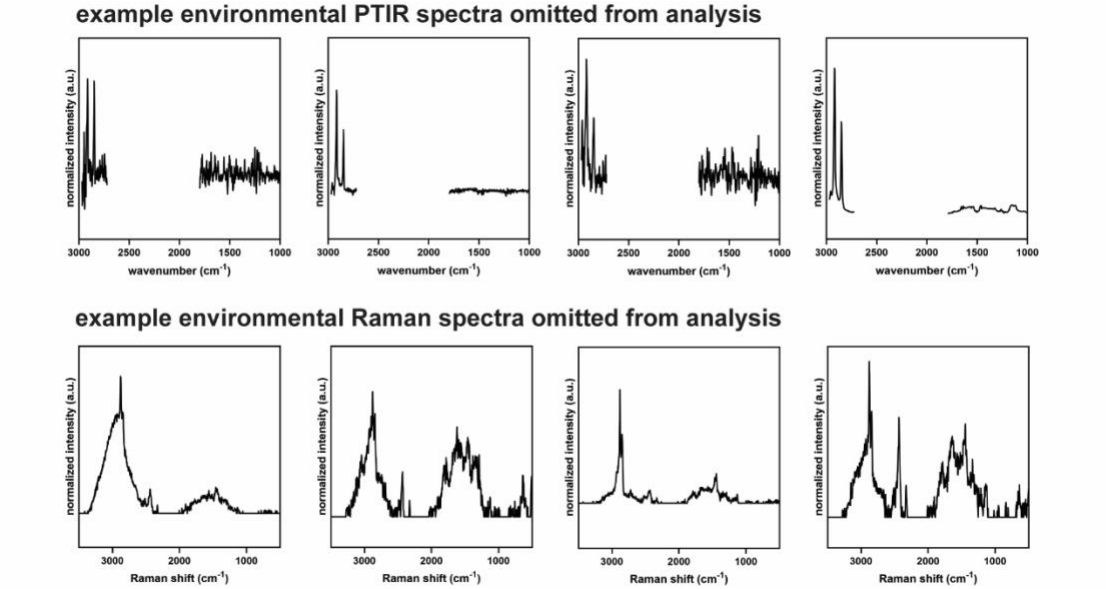

Figure S27. Example PTIR and Raman environmental spectra that had matched (HQI ≥ 0.7) to a high-density polyethylene (HDPE) spectrum in the mIRage MP library but was omitted from future analysis due to challenges with manual identification, such as low signal-to-noise ratio or fluorescent artefacts in the differentiable fingerprint range.

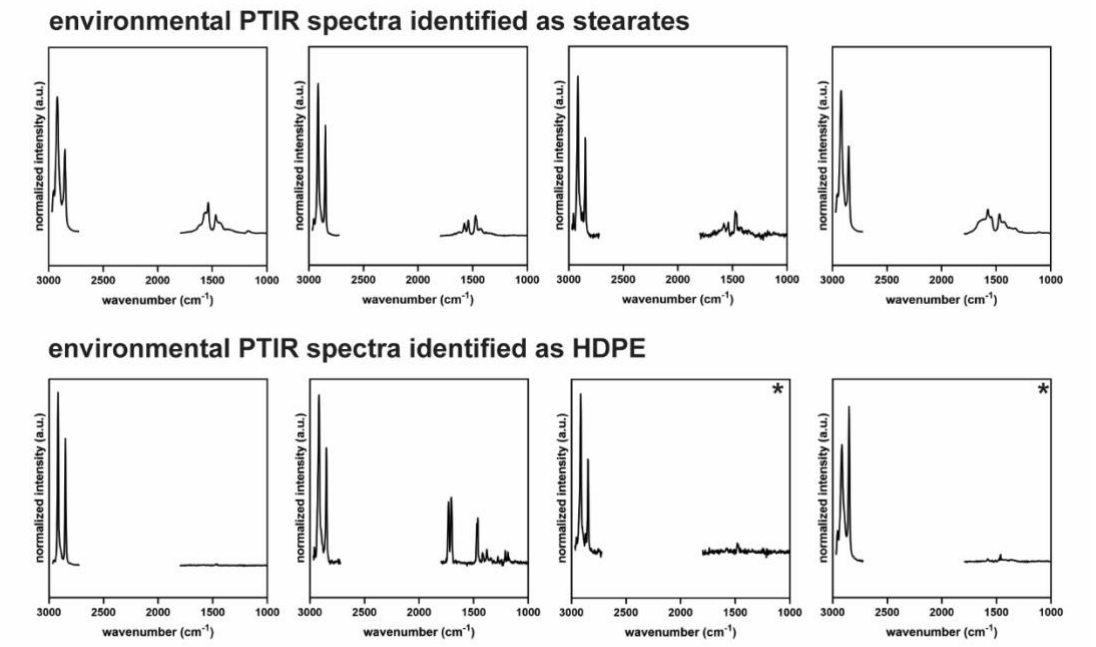

Figure S28. Example PTIR spectra manually identified as stearates or high-density polyethylene (HDPE). Asterisks indicate the two spectra in which the analyst and automated predictions did not agree, producing HDPE false negatives, likely due to the presence of noise in the region of stearate carboxylate vibrations.

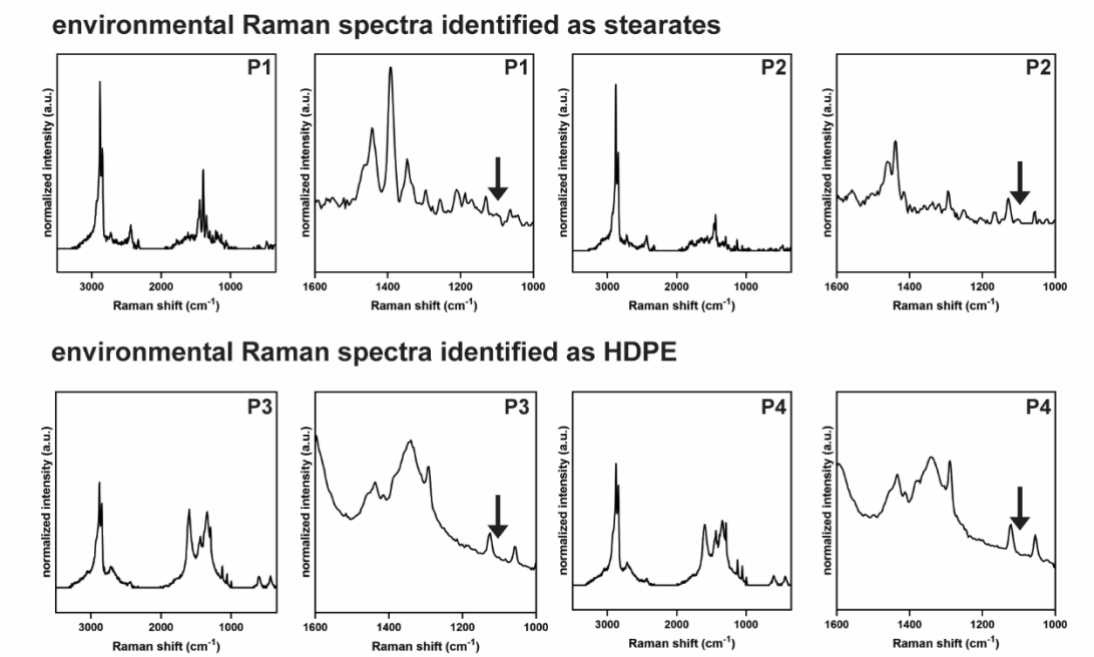

Figure S29. Example Raman spectra manually identified as stearates or high-density polyethylene (HDPE). The zoomed fingerprint region of the full spectrum is shown with arrow annotations marking the presence or absence of the peak at 1106 cm^{-1}.Spectra belonging to the same particle are marked with the same particle designator (e.g., P1).

Environmental HDPE and stearate optical images – To illustrate the small size of the particles analyzed in the environmental dataset and highlight the lack of distinguishing physical features between environmental HDPE and stearate particles, we present the optical images in Figure S30. As evidenced in the main text, optical differentiation between species is not a viable option to reduce MP false positives.

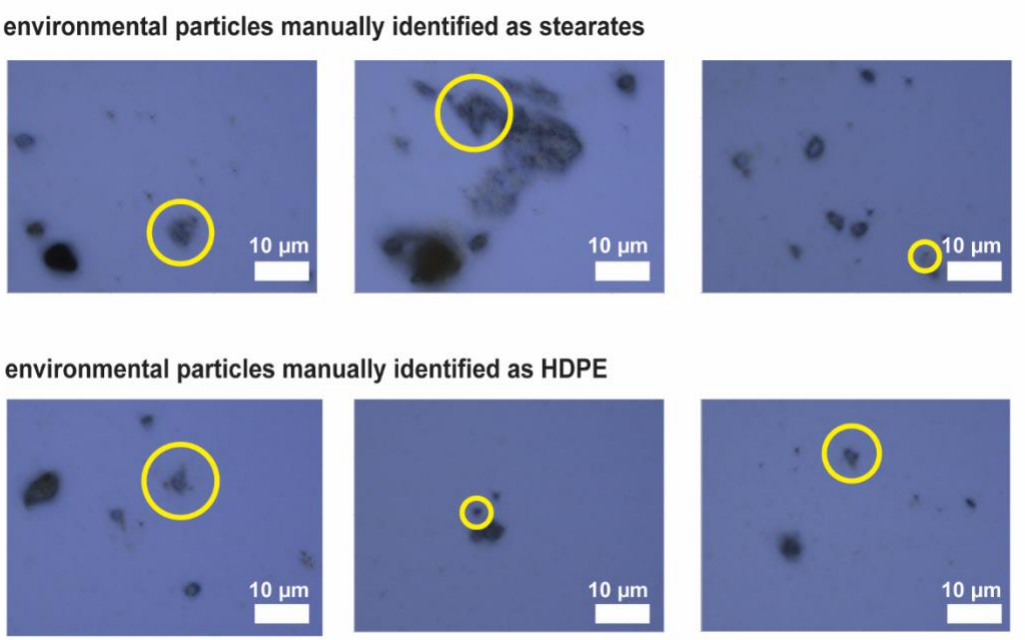

Figure S30. Visually indistinguishable images via mIRage 40X optical objective of manually identified stearates and high-density polyethylene (HDPE) particles from the environment. Particles of interest in the field of view are circled in yellow.

Practical notes on the application of automated methods – As in our suggested workflows, the PTIR spectra that had matched to an HDPE reference spectrum (HQI ≥ 0.7) were truncated to the extended fingerprint range (980–1800 cm^{-1}) and compared with PCC to mIRage HDPE and stearate reference spectra. The higher automated HQI dictated the identity of the automated PTIR prediction. Similarly, the Raman spectra that had matched to an HDPE reference spectrum (HQI ≥ 0.7) became a new CP test set for application of the same CP conditions employed in Section VIII.

As environmental data is understood to often suffer from reduced spectral quality when compared to lab-generated standard libraries,[22] it was expected for the results of our proposed automated solutions to show reduced performance. This phenomenon is observed in Figure S31, where comparing the HQI scores of the extended fingerprint region of the environmental PTIR data to the MP and stearate library reduced the magnitude separating the mean HQI to each identity is observed when compared to the library results shown in Figure 5. The reduced magnitude between the scores, as well as the occurrence of HDPE false negatives, reflects that the environmental data exhibit reduced SNR in the extended fingerprint ratio, likely related to environmental aging, allowing noise to be mistaken for true signal by the PCC similarity metric. Thus, visual analysis remains critical to the assessment of all automated identifications.

In a similar vein, CP using NN predicted both HDPE and stearate identities for over half the environmental spectra used in the test set. As described in Section VIII, the prediction set size can be modified by the analyst through tuning of the theoretical confidence guarantee, where a higher guarantee will lead to more identities in the prediction. As we employ a 95% theoretical confidence guarantee herein, it is expected that CP indicates uncertainty in the prediction by predicting both identities, prompting the user to conclude the identity of spectra through additional analysis.

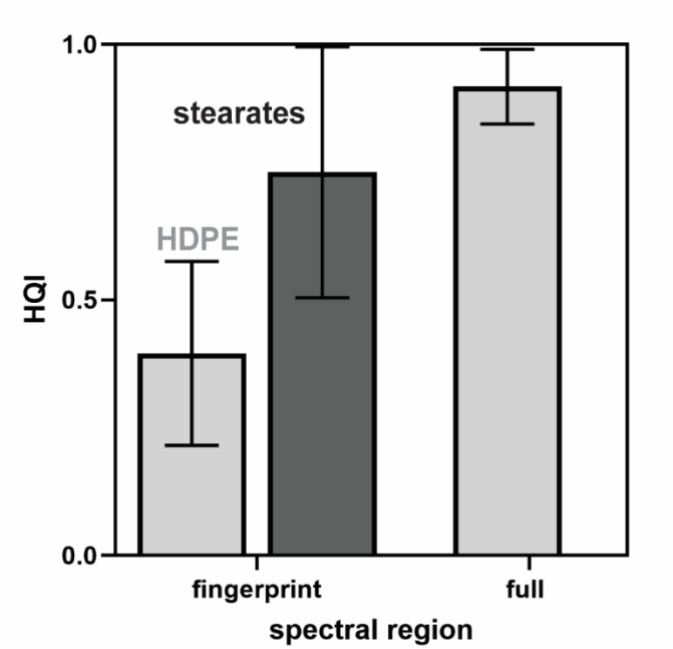

Figure S31. Depiction of mean HQI of the environmental PTIR spectra by spectral region when matched to stearate (dark gray) and high-density polyethylene (HDPE) reference spectra. Note that error bars represent standard deviation.

Investigating role of Raman data quality on CP performance – Due to simultaneous collection but separate preprocessing and exclusion pipelines, application of the data analysis routines for contaminated environmental data led to a processed dataset in which ten particles had both PTIR and Raman predictions of identity. Of these ten cases, three instances were found in which the automated and manual identity predictions by PTIR and Raman disagreed (Figure S32). Upon closer inspection, it appears that the environmentally-aged particles lacked a distinct 1106 cm^{-1} Raman peak attributed to stearate skeletal stretching (see Section XIII). This reduced Raman fingerprint spectral quality, which diminishes the distinction between HDPE and stearate spectra, likely led to the Raman misidentification.

To investigate how test data quality impacts CP performance for this application, we replaced the environmental Raman CP test set with a new test set built from mIRage reference library data.

Notably, this Raman dataset has improved spectral quality over the spectra observed in the environmental dataset (Figure S5, S6, and S7). Over 500 iterations, a new test set containing one HDPE example, five calcium stearate examples, three magnesium stearate examples, three sodium stearate examples, and five zinc stearate examples were randomly selected from the compiled reference libraries (see Section IV). The remaining reference spectra remained as a reference library, and all other CP conditions remained unchanged. From this experiment, we observed > 93% empirical confidence (i.e., proportion of instances in which the true identity was located in the prediction set) on average across identities, agreeing well with the theoretical 95% confidence guarantee (Figure S32). Additionally, the mean prediction set size (i.e., number of identities predicted for a spectrum) was less than two for all identities (Figure S33). We attribute this improved performance to increased spectral quality, where the presence or absence of the critical 1106 cm^{-1} peak is visible in all library Raman stearate spectra (Figure S6), but lacking in some environmental Raman stearate spectra (Figure S32). Thus, Raman spectral data quality, especially for environmentally aged particles, is critical to completely recovering contaminated datasets. Supplemental thermal or infrared data to support Raman-based investigations of stearate contamination in environmental MP datasets, specifically those at the lower size limits of analysis, will be valuable to accurate identification.

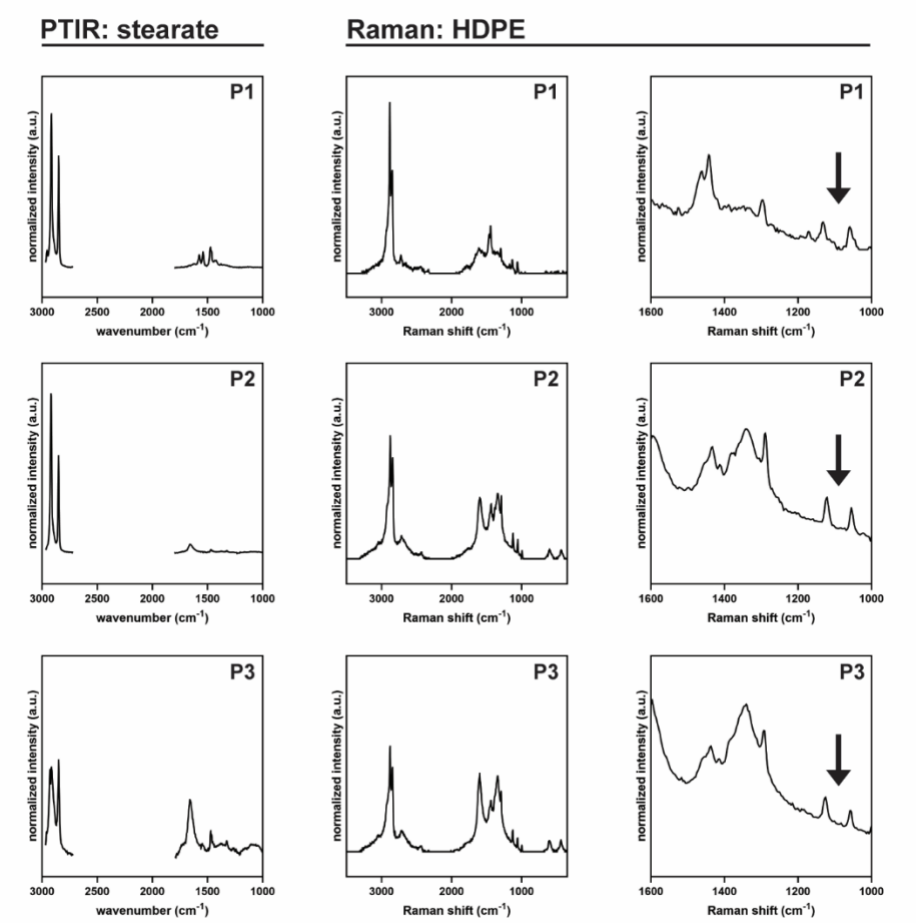

Figure S32. PTIR and Raman (full and zoomed view) spectra with conflicting identity predictions, wherein PTIR spectra were predicted to be stearate identity and Raman spectra were predicted to be HDPE identity. The lack of the distinguishing stearate peak at 1106 cm^{-1} is highlighted. Spectra belonging to the same particle are displayed in vertical rows, marked with the same particle designator (e.g., P1).

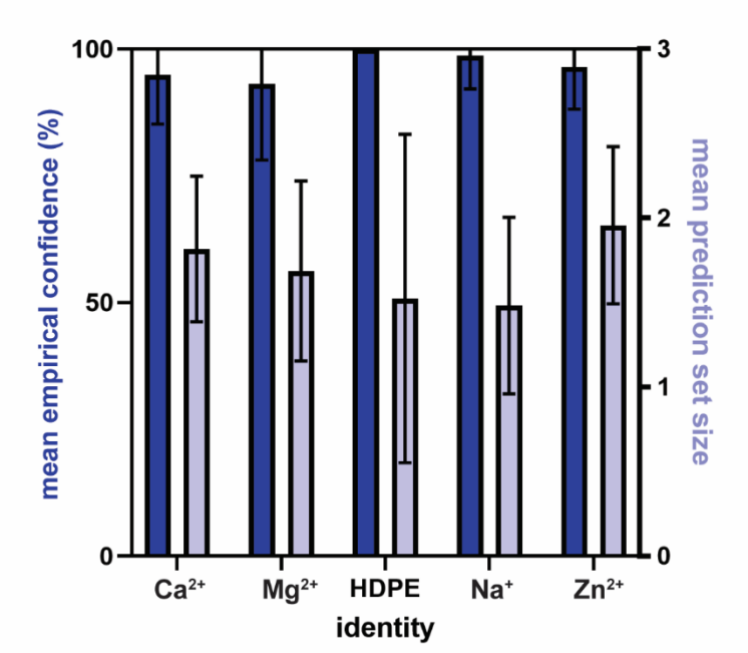

Figure S33. Mean empirical confidence and mean prediction set size for conformal prediction with mIRage HDPE and stearate Raman spectra. Stearate identities are displayed by their distinguishing cation.

X. Practical user-guide for differentiation workflow

Guidance for simplified application of differentiation workflows – The following simplified steps can be applied to the environmental dataset to reduce possible glove-based stearate contamination. While instructions for both automated and manual inspection are given, we present a simplified graphical workflow in Figures S34 and S35 for visual verification of infrared and Raman stearate contaminants. The manual verification guidance should benefit laboratories with reduced analytical capabilities.

Infrared Datasets:

1. Using MP reference libraries such as those provided, first use a similarity metric (e.g., PCC) to generate HQI scores of unknown spectral data to reference spectra.
2. Separate spectra that meet a chosen match criteria (e.g., HQI ≥ 0.7) for further investigation as “potential environmental MP” spectra.
3. For small datasets, visually flag infrared spectra that exhibit carboxylate peaks in the range of 1550–1580 cm^{-1}. For larger datasets for which visual inspection would be impractical, repeat step 1 with the “potential environmental MP” spectra from step 2 using a range inclusive of the differentiating carboxylate peaks but not C-H stretching peaks (e.g., 980–1800 cm^{-1}) with the provided stearate and MP reference libraries. Flag spectra with higher HQI to a stearate reference than a MP library.

4. Manually validate the flagged spectra as glove-based stearate contaminants or environmental MPs based on peak shape and position compared to provided reference spectra.

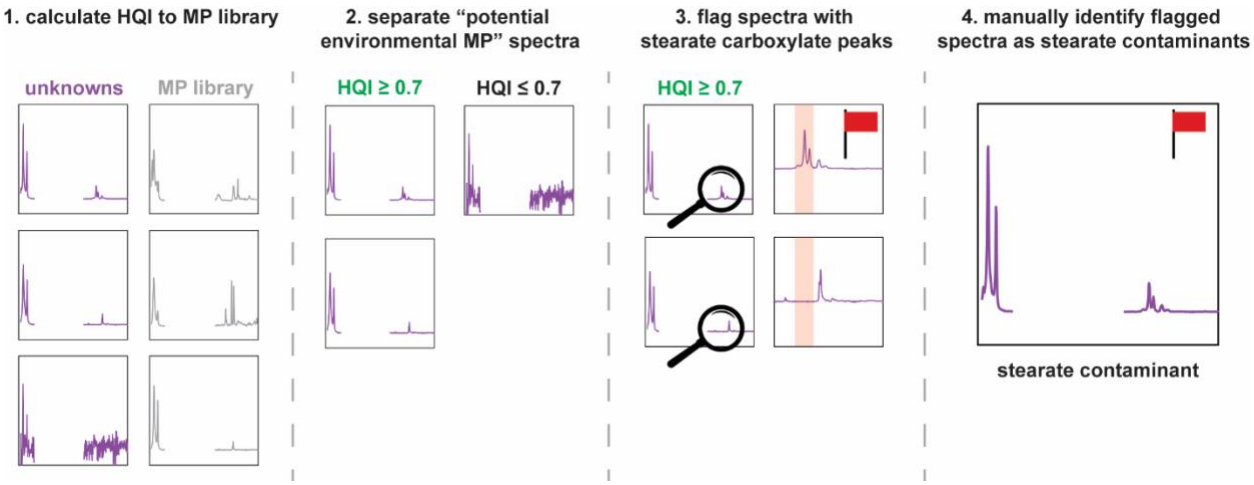

Figure S34. Visual workflow for manual verification of infrared spectra. Image credit: ValGraphic /AAVAA - stock.adobe.com

Raman Datasets:

1. Using MP reference libraries such as those provided, first use a similarity metric (e.g., PCC) to generate HQI scores of unknown spectral data to reference spectra.
2. Separate spectra that meet a chosen match criteria (e.g., HQI ≥ 0.7) for further investigation as potential environmental MP spectra.
3. For small, high SNR datasets, visually inspect the region 1000–1600 cm^{-1} to flag Raman spectra that exhibit a peak at 1416 cm^{-1} relating to HDPE skeletal C-C stretching as PE, and to flag Raman spectra that exhibit a peak at 1106 cm^{-1} relating to stearate C-C-C bending as stearate contaminants. For larger datasets or those with lower SNRs, for which visual inspection would be impractical, apply CP with the NN similarity metric to generate identity prediction sets using guaranteed confidence (e.g., 95%) and the provided MP and stearate reference libraries.
4. Interpret and visually confirm the prediction sets using the guidance below relating to the prediction set contents returned by CP.

   {stearate}: The spectral identity is likely glove-based stearate contamination. Ensure that the spectra have suitable SNR such that distinguishing stearate Raman peak at 1106 cm^{-1} is visible.

   {HDPE}: The spectral identity is likely HDPE. Ensure that the spectra have suitable SNR such that distinguishing HDPE Raman peak at 1416 cm^{-1} is visible, and that the distinguishing stearate Raman peak at 1106 cm^{-1} is not present.

{stearate, HDPE}: The spectral identity is inconclusive. Collect additional data (e.g., IR, thermal analysis, higher SNR acquisition) to support an identification subject to manual review.

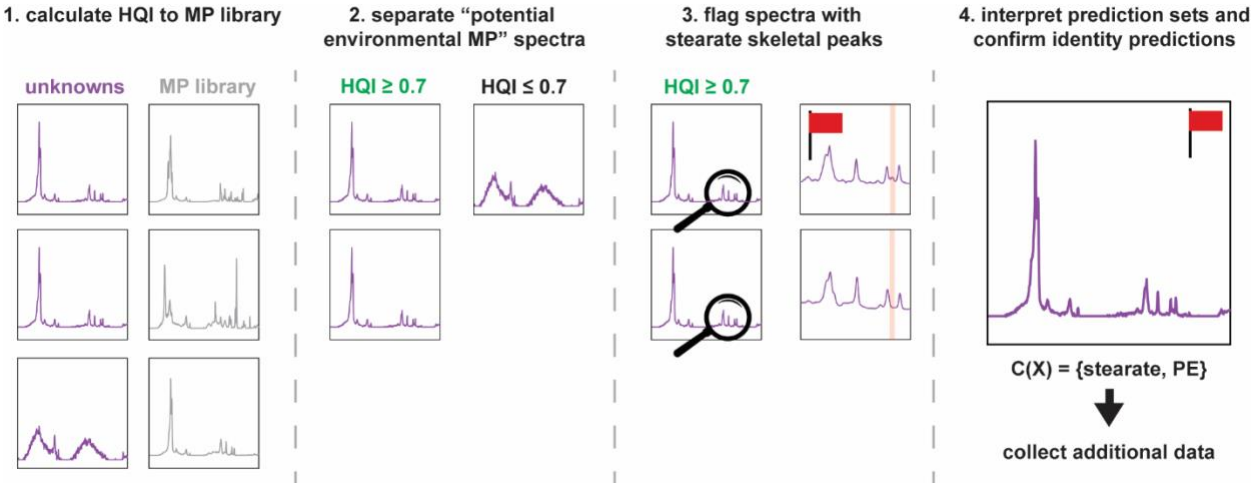

Figure S35. Visual workflow for manual verification of Raman spectra. Image credit: ValGraphic /AAVAA - stock.adobe.com

XI. Traditional topmost HQI-based spectral matching results

Spectral identity indicated by library matching – To determine the most common identities predicted by traditional, topmost HQI-based spectral matching methodologies using both stearate and MP standard libraries collected on the mIRage O-PTIR + Raman system, the number of spectral matches to each identity per substrate was first determined. Next, the quantity of spectra matched to each identity in the reference library were averaged between the two substrates of a singe glove brand. The average proportion of each spectral identity between duplicate samples of the same glove brand was then calculated.

Calcium stearate was indicated to be the major predicted identity by PTIR and Raman when the residue data was compared to the stearate standard spectral reference library and spectra with topmost HQI ≥ 0.7 were considered as spectral matches (Figure S36). Because the distinguishing carboxylate stretch is Raman inactive, variation in identities indicated by Raman spectral matching speaks to small spectral variations in noise or artefacts dictating the identity of topmost HQI. The identities indicated by PTIR spectral matching provide more information on likely mold release agents used in laboratory glove manufacturing, as variations in the fingerprint region of the infrared stearate reference spectra are observed (Figure S6).

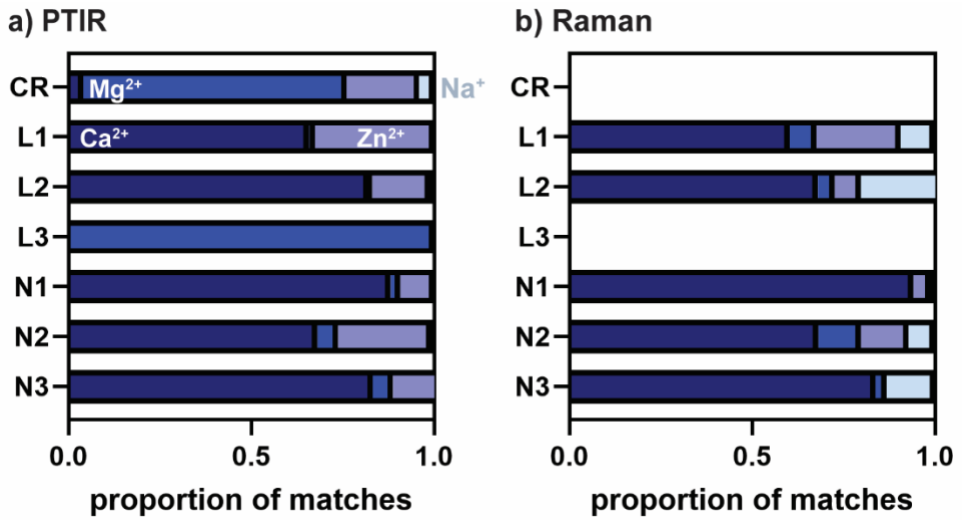

Figure S36. Average proportion of matched spectral identity of particles released from dry contact with laboratory gloves by considering (a) PTIR and (b) Raman spectra matched to the stearate reference library. Stearate identities are represented by their distinguishing cation. Note that CR and L3 glove types did not produce matches (HQI ≥ 0.7) by Raman spectroscopy analysis.

When only microplastic libraries were used to perform traditional topmost HQI-based matching practices, HDPE was the dominant identity returned to both PTIR and Raman data (Figure S37). Unsurprisingly, higher variation in average identity proportion is observed for PTIR spectra than Raman spectra, likely due to higher spectral variability in the PTIR spectra.

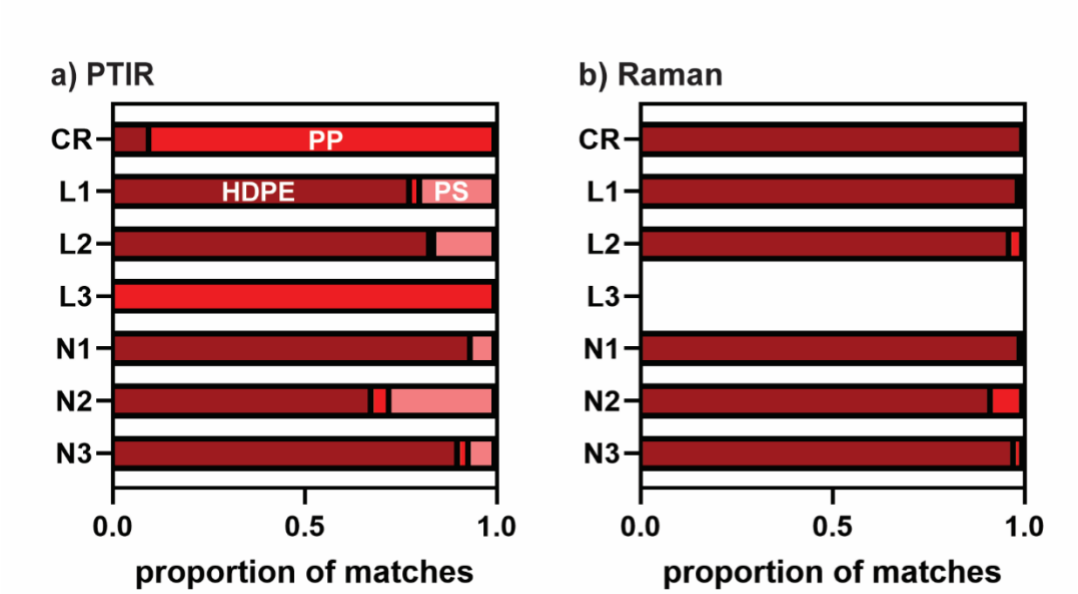

Figure S37. Average proportion of matched spectral identity of particles released from dry contact with laboratory gloves by considering (a) PTIR and (b) Raman spectra matched to the microplastic reference library. Note that the L3 glove type did not produce matches (HQI ≥ 0.7) by Raman spectroscopy data analysis.

While stearate, and thus MP, identities accounted for most of the non-volatile residues that were imparted from dry contact with laboratory gloves (Figure S38), it is valuable to note that non-volatile particles were released by all glove types evaluated herein (Figure S39).

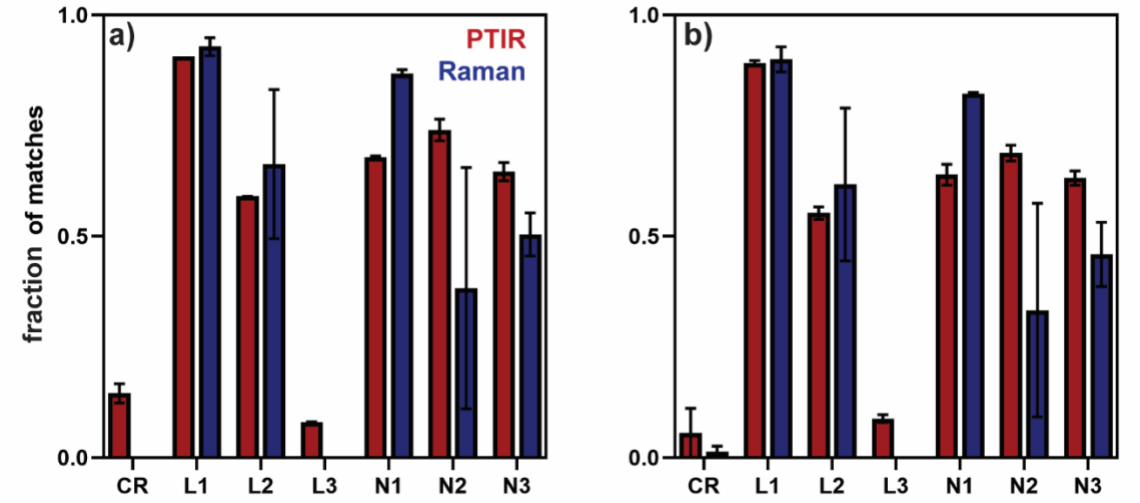

Figure S38. Fraction of matches (HQI ≥ 0.7) from all PTIR and Raman spectra of particles from laboratory gloves when using the (a) stearate or (b) microplastic reference library.

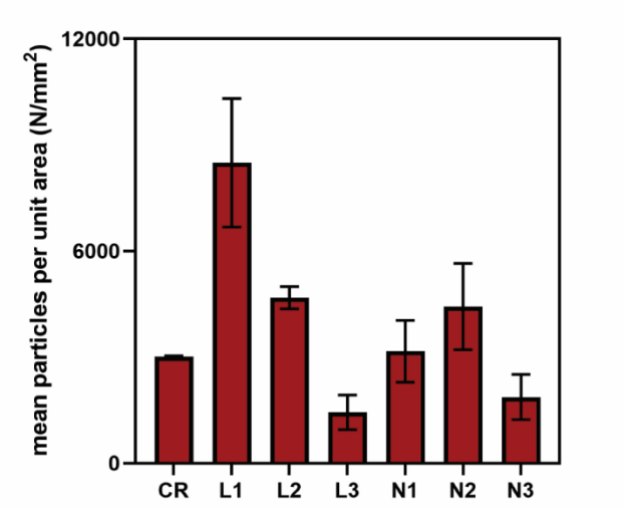

Figure S39. Mean quantity of particles, including stearate and non-stearate identities, released from dry contact with laboratory gloves per glove sample.

Normalizing results to area and performing blank correction – To compare the quantity of stearates or falsely identified MPs per substrate area, the number of matches (HQI ≥ 0.7) for either the stearate or MP library was first tallied for each substrate. The quantity was normalized to area by dividing the number of matches per substrate (including the duplicate procedural blanks) by the area of substrate analyzed for PTIR and Raman spectral collection according to equation S7, where m_1 and m_2 refer to the number of matches on substrate 1 and 2, respectively.

$$\bar{m} = \frac{(m_1) * (m_2)}{2} \quad (S7)$$

To obtain a mean number of matches per unit area, the mean number of matches was divided by the sum of analyzed area on substrate 1 and 2 (a_1 and a_2, respectively) and values were extrapolated to mm^2 surface areas according to equation S8.

$$\frac{\bar{m}}{mm^2} = \frac{\bar{m}}{(a_1 + a_2)\ \mu m^2} * \frac{1 \cdot 10^6\ \mu m^2}{1\ mm^2} \quad (S8)$$

Next, the quantities per unit area were averaged between duplicate samples of the same type to produce a mean quantity of library matches per unit area. Finally, the mean quantity of matches observed for the procedural blanks was subtracted from each mean quantity of matches observed for the glove samples. Any negative value was adjusted to zero and the standard deviation between the duplicate substrates was calculated.

Of all analyzed particles on the procedural blanks, processing the spectra gave five PTIR MP false positives, zero Raman MP false positives, two PTIR stearate matches, and zero Raman stearate matches.

Calculating confidence intervals for each glove and signal pair – The goal of this study was not to prescribe a glove that should be used for all future MP analysis, and therefore the use of power and/or advanced error calculations may complicate the message that most laboratory gloves will release stearates to a contacted surface. However, the 95% confidence interval was obtained for each glove and signal pair using equation S9, where CI is the confidence interval, $\bar{x}$ is the mean, z is the 95% z-score (1.96), s is the standard deviation, and n is the sample size. Here, n = 6 (two substrates, each with three regions of observation). Results in Figure S40 consider matches to both stearate and MP libraries.

.

$$CI = \bar{x} \pm z\frac{s}{\sqrt{n}} \tag{S9}$$

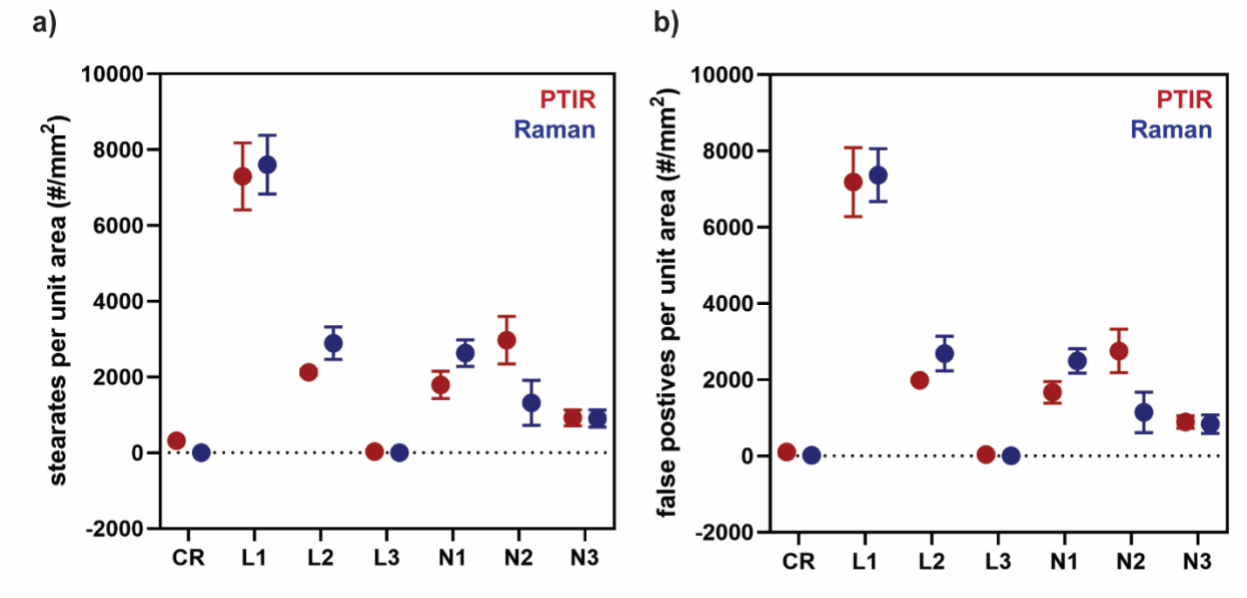

Figure S40. Mean and 95% confidence intervals for imprinted particle PTIR and Raman signals matching (HQI ≥ 0.7) to (a) mIRage stearate and (b) mIRage MP libraries.

Investigating spectral similarity of stearate and microplastic identities – To investigate the utility of the stearate reference library, the preprocessed residue spectral data was library matched to the combined stearate and MP reference libraries collected from the mIRage system. To illustrate the proportion and number of glove-imprinted residue spectra that switched or remained consistent between an identity predicted by topmost HQI when only using MP libraries (labels shown in red on the left y-axis) versus when using a combined MP and stearate spectral library (labels shown in blue on the x-axis), we present the heat maps in Figure S41 and Figure S42.

For both PTIR and Raman spectra, HDPE is the dominant false positive identity observed. While some utility in reducing false positives by topmost HQI is evident for the PTIR stearate library, shown by the 58% of spectra previously identified as HDPE moving to calcium stearate labels when the updated libraries are introduced, there remains disagreement between the identities of the remaining spectra. As evidenced in the main text, the similarity between topmost HQI scores of the PTIR data illustrates that reliance on HQI scores alone cannot indicate glove contamination.

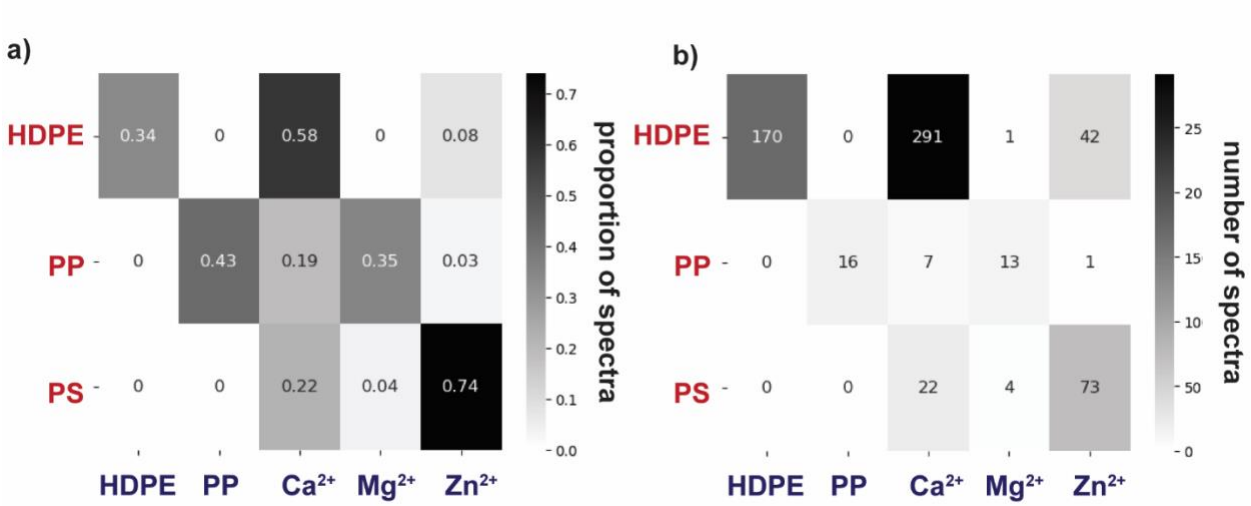

Figure S41. Heat map representing (a) the proportion of PTIR spectra and (b) the number of PTIR spectra that switched topmost match identity from an original microplastic library match (red) to an updated microplastic and stearate library match (blue). Stearate identities are represented by their distinguishing cation.

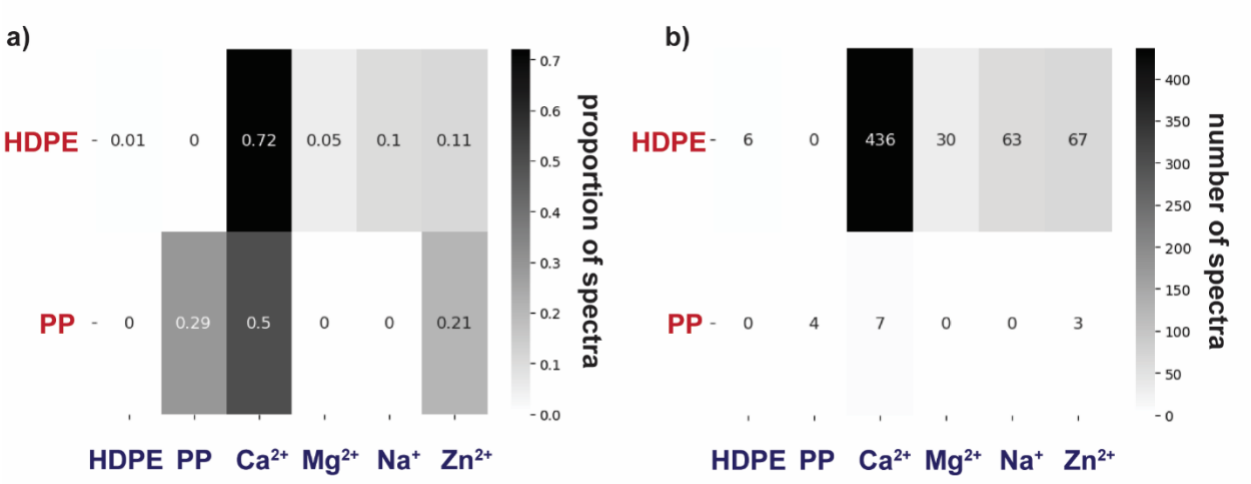

Figure S42. Heat map representing (a) the proportion of Raman spectra and (b) the number of Raman spectra that switched topmost match identity from an original microplastic library match (red) to an updated microplastic and stearate library match (blue). Stearate identities are represented by their distinguishing cation.

The stearate library is more effective when used with Raman spectral data, which is surprising, given that the reference spectra of HDPE and calcium stearate are identical at first glance (Figure S43). Similar to the explanation provided in the main text, it is likely small differences in SNR and baseline noise impacting topmost HQI between these highly similar spectra, indicating that HQI is not an effective method to distinguish between these species. Indeed, the difference in topmost HQI between stearate and MP labels for the same unidentified spectra is only 0.01 ± 0.03 for PTIR spectra and 0.02 ± 0.02 for Raman data (Figure S44), and false positive matches to MP identities return HQI scores above 0.9 for both PTIR and Raman spectra, indicating near complete agreement with incorrect chemical identities (Figure S45).

As a previous study indicated that distinguishment between sodium stearate and PE was possible by topmost HQI methods used with FTIR methods,[1] we hypothesize that the size of the particles analyzed in each study may play a role in the efficacy of HQI-based spectral matching practices. For instance, the spectra analyzed in the Witzig et al. article originated from film-like coverings on a filter surface, likely leading to higher SNR than observed herein, where the spectra obtained from dry glove contact originated from single-particles of mean 1.6 ± 0.8 µm projected area diameter (Figure S46).

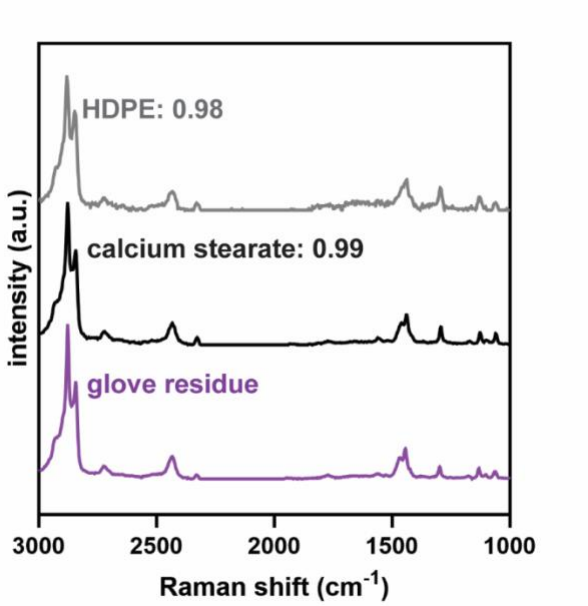

Figure S43. Raman spectra of glove residue alongside stearate and high-density polyethylene (HDPE) reference spectral match with topmost HQI. Noise visible in the HDPE spectrum is hypothesized to lead to lower HQI than observed with calcium stearate.

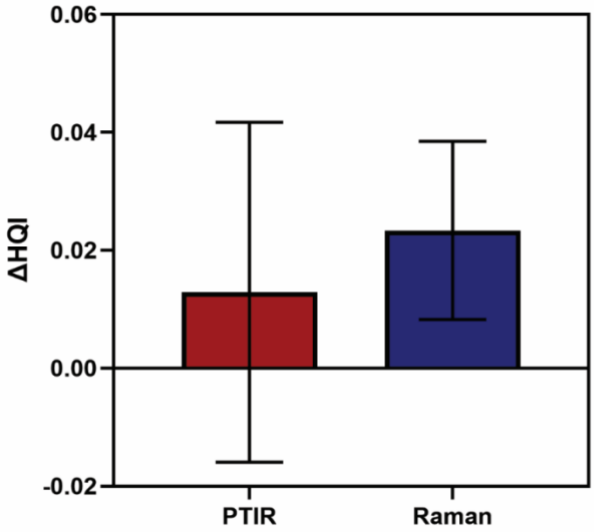

Figure S44. Magnitude of difference in HQI between topmost stearate identity and topmost microplastic identity (i.e., $HQI_{stearate} - HQI_{HDPE}$) returned by individual library searches for PTIR and Raman residue spectra. Note that error bars represent standard deviation between HQI scores.

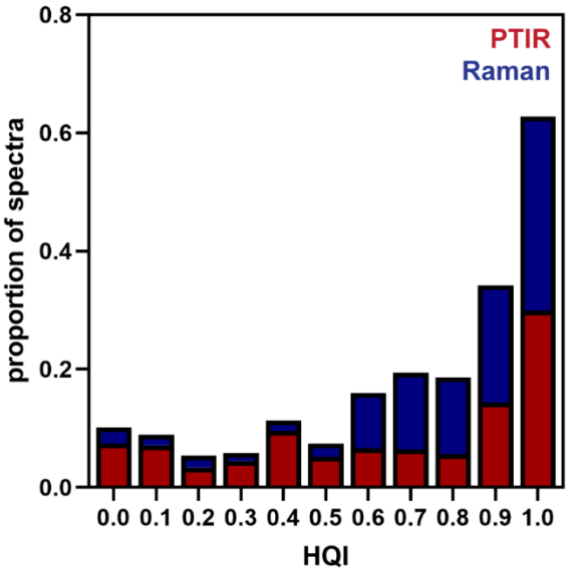

Figure S45. Distribution of topmost HQI scores to microplastic references (false positives) from glove residue spectra.

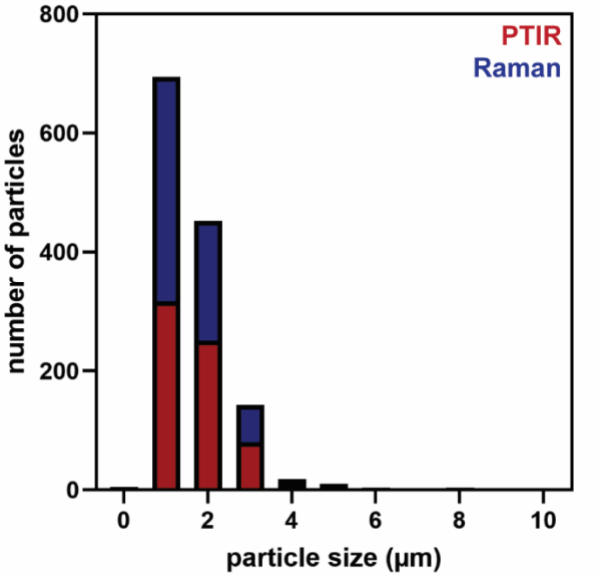

Figure S46. Combined size (from featurefindIR® measurements of projected area diameter) distribution of all stearate library matches (HQI ≥ 0.7) from all glove samples by PTIR and Raman signals. Mean particle size was calculated to be 1.6 ± 0.8 µm.

XII. Comparing topmost HQI-based results using alternate libraries

Herein, reference libraries were composed of single particle measurements of stearates and MPs (to best mimic unidentified spectra from the same system), as opposed to the bulk µ-FTIR libraries employed by pre-Witzig et al. To compare the behavior of automated topmost HQI-based library matching practices with different libraries, we used the "FTIR library of plastic particles" (FLOPP) and "FTIR library of plastic particles sourced from the environment (FLOPP-e)" libraries as reference spectra for the glove residue data.[23] The spectra from the FLOPP and FLOPP-e libraries were transformed according to the Beer-Lambert law (equation S4).[24] All cotton examples were removed from the libraries prior to matching with the workflow described in Section V such that only the quantity of MP false positives were evaluated.

As seen in Figure S47, the number quantity of MP false positives remains relatively consistent between the evaluated libraries. However, when the FLOPP and FLOPP-e MP reference spectra are combined with the stearate libraries collected herein, a much more drastic impact on the distinguishment of spectral identity is observed for the PTIR data than with the mIRage MP libraries (Figure S48). Compared to Figure S41, the efficacy of the stearate library when used with the FLOPP and FLOPP-e reference library is much improved. However, the difference in instrumentation and analysis method (PTIR versus FTIR), as well as particle size and thus SNR, likely influences the HQI score to preferentially match spectra with similar artefacts, falsely inflating the trend observed for matching with FTIR libraries. Rather than distinguishing particles based on chemical identity, the PTIR spectra preferentially match based on similar reference data (i.e., single-particle PTIR stearate library versus bulk FTIR MP library).

The explanation of differences in analytical method and spectral artefacts influencing topmost HQI match is further evidenced by comparison of matching behavior with the imprinted Raman data when the open-source libraries of "Spectral Library of Plastic Particles" (SLOPP) and "Spectral Library of Plastic Particles Aged in the Environment" (SLOPP-e) are used in conjunction with the mIRage Raman stearate library (Figure S49).[25] Although the Raman spectra of HDPE and calcium stearate are identical by routine visual analysis, the HQI-based matching routine indicated higher topmost HQI matches to calcium stearate than HDPE for all residue data. Again, it is the influence of data similarity between residue spectra and stearate reference spectra collected with the same instrument and parameters rather than any distinguishment of chemical identity that dominates topmost HQI-based identification routines. When insubstantial changes in topmost HQI are treated as indications of spectral identity, the underlying influence of spectral artefacts and SNR similarity are overlooked.

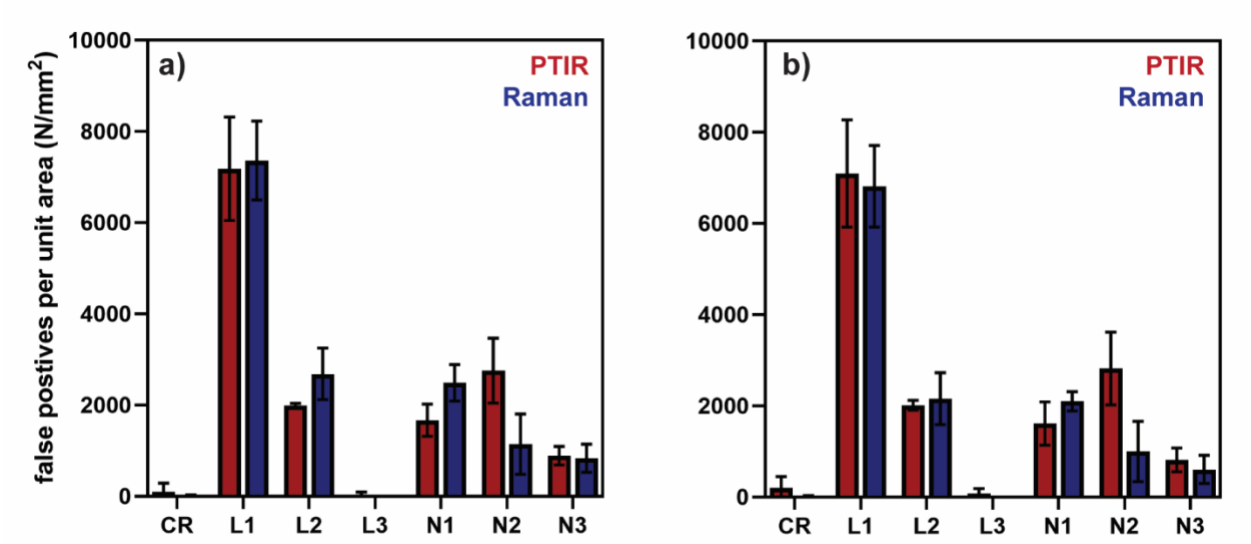

Figure S47. Quantity of PTIR and Raman (a) mIRage microplastic and (b) FLOPP/e and SLOPP/e microplastic matches per unit area for each glove type. Note that error bars represent standard deviation between two replicate samples.

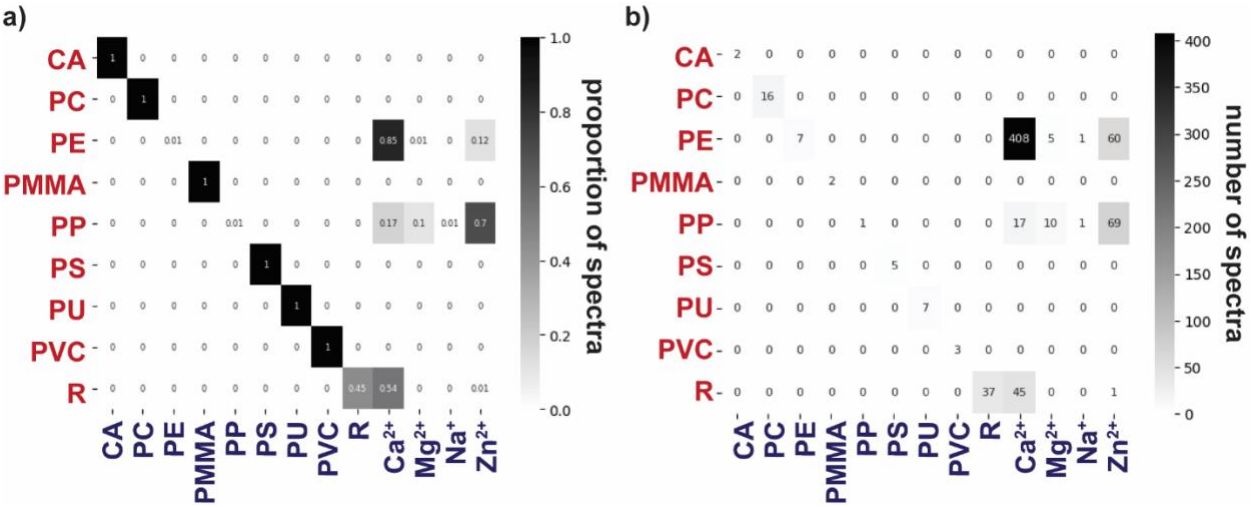

Figure S48. Heat map representing (a) the proportion of PTIR spectra and (b) the number of PTIR spectra that switched topmost match identity from an original microplastic library match (red) to an updated microplastic and stearate library match (blue). Stearate identities are represented by their distinguishing cation. CA refers to cellulose acetate, PC refers to polycarbonate, PMMA refers to poly(methyl methacrylate), PS refers to polystyrene, PU refers to polyurethane, PVC refers to poly(vinyl chloride), and R refers to rubber. Note that the FLOPP/e libraries do not detail PE density.

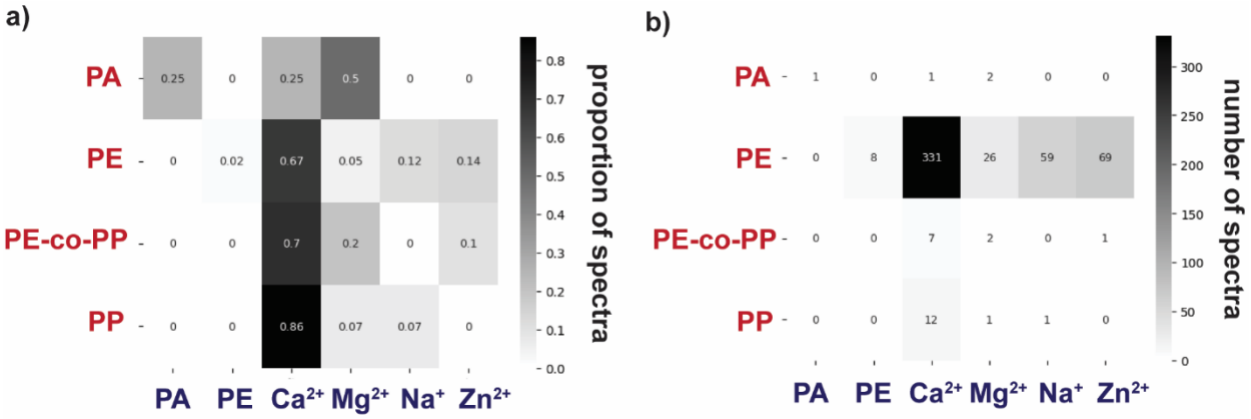

Figure S49. Heat map representing (a) the proportion of Raman spectra and (b) the number of Raman spectra that switched topmost match identity from an original microplastic library match (red) to an updated microplastic and stearate library match (blue). Stearate identities are represented by their distinguishing cation. PA refers to polyacrylate and PE-co-PP refers to polyethylene-co-polypropylene. Note that the SLOPP/e libraries do not detail PE density.

XIII. Distinguishing stearate and polyethylene Raman spectra

Additional Raman spectra with higher resolution were collected on the mIRage O-PTIR + Raman system. Using the reference library samples of HDPE and calcium stearate (selected due to their high spectral similarity as shown in Figures S40), Raman spectra were acquired at a resolution of 3.4 cm^{-1} using 0.5% laser power and ten averages of 10 s integrations. Raman signal was collected from 170–4000 cm^{-1}. In addition to presenting the two distinct peaks graphically in the main text, a peak assignment table that highlights the distinguishing region 1000–1600 cm^{-1} is presented in Table S3.

HDPE peak location (cm^{-1})	calcium stearate peak location (cm^{-1})	vibrational attribution	reference number
1460	1458	δ(CH2)	26, 27
1440	1438	δ(CH2)	23, 24
1416	-	ω(CH2)	24, 28
1295	1293	δ(CH2)	23, 24
1130	1129	v_s(C–C)	23, 24
-	1106	ν(C-C) + δ(C-C-C)	23, 29
1062	1061	v_{as}(C–C)	23, 24

Table S3. Peak location, vibrational attribution, and reference number for the distinction of high-density polyethylene (HDPE) from calcium stearate Raman spectra. Blue cells indicate distinguishable peaks present in only one spectrum.

XIV. References

(1) C. S. Witzig, C. Földi, K. Wörle, P. Habermehl, M. Pittroff, Y. K. Müller, T. Lauschke, P. Fiener, G. Dierkes, K. P. Freier, and N. Zumbülte, *Environ. Sci. Technol.*, 2020, **54**, 12164–12172.
(2) J. J. Hermans, K. Keune, A. van Loon, M. J. N. Stols-Wilcox, R. W Corkery, and P. D. Iedema, *Proceedings of ICOM-CC 17th Triennial Conference*, Melbourne, Australia, 2004.
(3) L. Barbeş, C. Rădulescu, and C. Stihi, *Rom. Rep. Phys.* 2014, **66**, 765–777.
(4) J. R. Macairan, A. Saherwala, F. Li, F. Monteil-Rivera, N. Tufenkji, *Environ. Sci. Technol.* 2025, **59**, 15612–15622
(5) R. L. Parham, A. Ayala, L. Meagher, M. E. Clough, E. Ochoa Rivera, J. Shi, A. Tewari, A. J. McNeil, and A. P. Ault, *Anal. Chem*., 2025, **97**, 18136–18143.
(6) J. S. Böke, J. Popp, and C. Krafft, Sci. Rep. 2022, 12, 18785.
(7) R. J. Barnes, M. S. Dhanoa, and S. Lister, S. *J. Appl. Spectrosc*. 1989, **43**, 772–777.
(8) L. I. Rudin, S. Ocher, and E. Fatemi, *Phys. D: Nonlinear Phenom*. 1992, **60**, 259–268.
(9) IUPAC Gold Book 'limit of detection', https://goldbook.iupac.org/terms/view/L03540, (accessed 2025-04-25).
(10) W. Cowger, Z. Steinmentz, A. Gray, K. Munno, J. Lynch, H. Hapich, S. Primpke, H. De Frond, C. Rochman, and O Herodotou, *Anal. Chem.*, 2021, **93**, 7543–7548.
(11) J. Zhao, H. Lui, D. I. McLean, and H. Zeng, *Appl. Spectrosc.* 2007, **61**, 1225–1232.
(12) D. M. Jr., Sublett, E. Sendula, H. M. Lamadrid, M. Steele-MacInnis, G. Spiekermann, and R. J. Bodnar, *J. Raman Spectrosc.* 2021, **52**, 750–769.
(13) M. E. Clough, E. Ochoa Rivera, R. L. Parham, A. P. Ault, P. M. Zimmerman, A. J. McNeil, and A. Tewari, *Environ. Sci. Technol.*, 2024, **58**, 21740–21749.
(14) D. Schymanski, B. R. Oßmann, N. Benismail, K. Boukerma, G. Dallmann, E. von der Esch, D. Fischer, F. Fischer, D. Gililand, K. Glas, T. Hofmann, A. Käppler, S. Lacorte, J. Marco, M. E. L. Rakwe, J. Weisser, C. Witzig, N. Zumbülte, and N. P. Ivleva, *Anal. Bioanal. Chem*., 2021, **413**, 5969–5994.
(15) J. Delgado-Gallardo, G. L. Sullivan, P. Esteban, Z. Wang, O. Arar, L. Zi, T. M. Watson, and S. Sarp, *ACS EST Water,* 2021, **1**, 748–764.
(16) W. Yagoubi, A. Abdelhafidi, M. Sebaa, and S. F. Chabira. *Polym. Test*. 2015, **44**, 37–48.
(17) G. Grause, M.-F. Chien, and C. Inoue. *Polym. Degrad. Stabil.* 2020, **181**, 109364.
(18) V. Vovk, A. Gammerman, and C. Saunders, *Proceedings of the Sixteenth International Conference on Machine Learning*, Bled, 1999.
(19) V. Vovk, A. Gammerman, and G. Shafer, *Algorithmic Learning in a Random World*, Springer, New York, NY, 2005.
(20) G. Shafer, and V. Vovk, *J. Mach. Learn. Res.* 2008, **9**, 371–421.
(21) D. K.Ott, and T. M. Peters, *Aerosol Sci. Technol*. 2008, **42**, 299–309.
(22) G. Binda, G. Kalčíková, I. John Allan, R. Hurley, R. Rødland, D. Spanu, and L. Nizzetto, *TrAC, Trends Anal. Chem.*, 2024, **172**, 117566.
(23) H. De Frond, R. Rubinovitz, and C. M. Rochman, *Anal. Chem*. 2021, **93**, 15878–15885.
(24) F. Herb, M. Boley, and W-K. Fong, *J. Hazard. Mater.* 2025, **487**, 136989.
(25) K. Munno, H. De Frond, B. O'Donnell, and Rochman, C. M. *Anal. Chem*. 2020, **92**, 2443–2451.
(26) L. Robinet, and C. M. Corbiel, *Stud. Conserv*., 2003, **48**, 23–40.
(27) V. Nava, M. L. Frezzotti, and B. Leoni, *Appl. Spectrosc*., 2021, **75**, 1341–1357.
(28) G. R. Strobl, and W. Hagedorn, *J. Polym. Sci.*, 1978, **16**, 1181–1193.
(29) M. de Veij, P. Vandenabeele, T. De Beer, J. P. Remon, L. Moens, *J. Raman Spectrosc.*, 2009, **40**, 297–307.